Supplementary Material (ESI) for CrystEngComm

ELECTRONIC FEATURES AND HYDROGEN BONDING CAPACITY OF THE SULFUR ACCEPTOR IN THIOUREIDO-BASED COMPOUNDS. EXPERIMENTAL CHARGE DENSITY STUDY OF 4-METHYL-3-THIOSEMICARBAZIDE

Bojana M. Francuski, Sladjana B. Novaković, Goran A. Bogdanović,
VINČA Institute of Nuclear Sciences, Laboratory of Theoretical Physics and Condensed Matter Physics, PO Box 522, 11001 Belgrade, Serbia

ELECTRONIC SUPPLEMENTARY INFORMATION

Content

Table S1. Experimental net atomic charges and atomic volumes from QTAIM partitioning of the electron density for MeTSC[a].

Atom	q(Ω)	V_{tot} (Å^3)
S1	−0.15 −0.20	28.59 30.06
N1	−0.68 −0.81	14.87 15.87
N2	−1.10 −0.98	14.25 13.92
N3	−1.15 −1.16	12.31 13.84
C1	0.91 0.86	6.90 7.17
C2	−0.10 0.08	12.90 11.23
H2	0.47 0.45	3.73 3.43
H3	0.44 0.40	2.98 2.95
H11	0.36 0.38	4.49 4.42
H12	0.40 0.41	3.93 3.90
H21	0.34 0.14	6.26 6.19
H22	0.01 0.24	7.20 6.14
H23	0.30 0.17	5.74 5.69

[a] The first line for each atom gives values from molecule A, and second line values from molecule B.

Table S2. Topological proprieties of non-covalent interactions involving S atom in SalTSC.

D–H···A	D–H[a]	H···A[a]	D–H···A[b]	ρ_{bcp}[c]	$\nabla^2\rho_{bcp}$[d]	d_1[e]	d_2[e]	H_{bcp}[f]	G_{bcp}[f]	V_{bcp}[f]	ΔrH+ΔrS[g]
N2−H2n···S1[i]	0.966(9)	2.459(10)	168.5(8)	0.093(17)	1.27(2)	1.597	0.862	5.54	28.97	−23.43	0.862
C7−H7···S1[ii]	1.068(8)	3.001(8)	125.4(6)	0.030(2)	0.42(1)	1.891	1.186	2.95	8.61	−5.66	0.378
C2−H2···S1[i]	1.057(8)	2.940(8)	140.8(6)	0.038(4)	0.51(2)	1.845	1.125	3.26	10.55	−7.29	0.537
C5−H5···S1[iii]	1.081(9)	3.118(9)	115.9(6)	0.032(2)	0.36(1)	1.995	1.278	2.36	7.43	−5.07	0.498
C4−H4···S1[iii]	1.082(7)	3.086(7)	114.4(4)	0.039(2)	0.46(1)	1.855	1.269	2.79	9.78	−6.99	0.602
N3−H3n1···S1[iv]	0.991(9)	2.963(10)	120.5(7)	0.035(2)	0.47(1)	1.851	1.216	3.13	9.76	−6.64	0.578

[a] Units of Å. [b] Units of º. [c] Units of e Å^{-3}. [d] Units of e Å^{-5}. [e] $d1$ and $d2$ are the distances (Å) of the bcp to the nuclei. [f] Units of kJ mol^{-1} bohr^{-3}; [g]Interpenetration of van der Waals's spheres of donor and acceptor atoms (Å),. Symmetry codes: [i]1.5−x,0.5−y,1−z; [ii]x,y, −1+z; [iii]1.5−x,-0.5+y,0.5−z; [iv]x,1−y, −0.5+z.

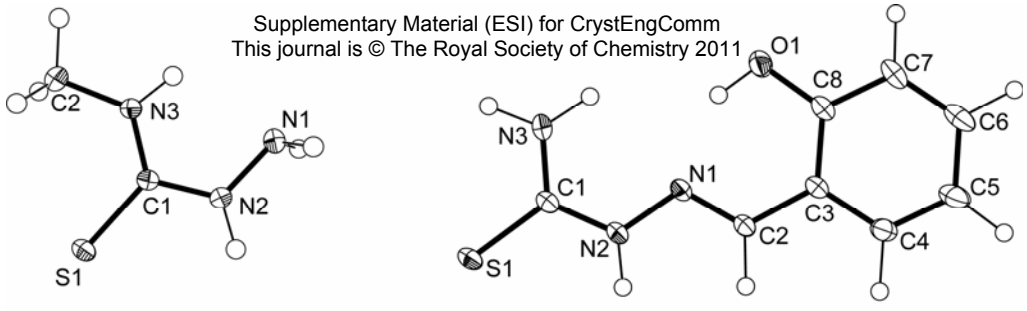

Figure S1. Crystal structures of MeTSC (left) and SalTSC (right).

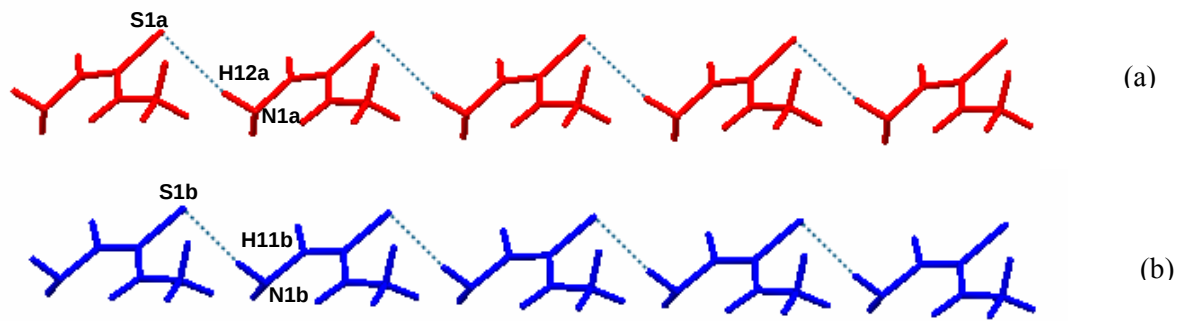

Figure S2. The chains of A and B molecules (given in red and blue, respectively) oriented in the same way as an illustration of mutual conformational similarity. (a) The chain composed of A molecules formed by the N1a−H12a···S1a interactions. (b) The chain of B molecules formed by the N1b−H11b···S1b interactions.

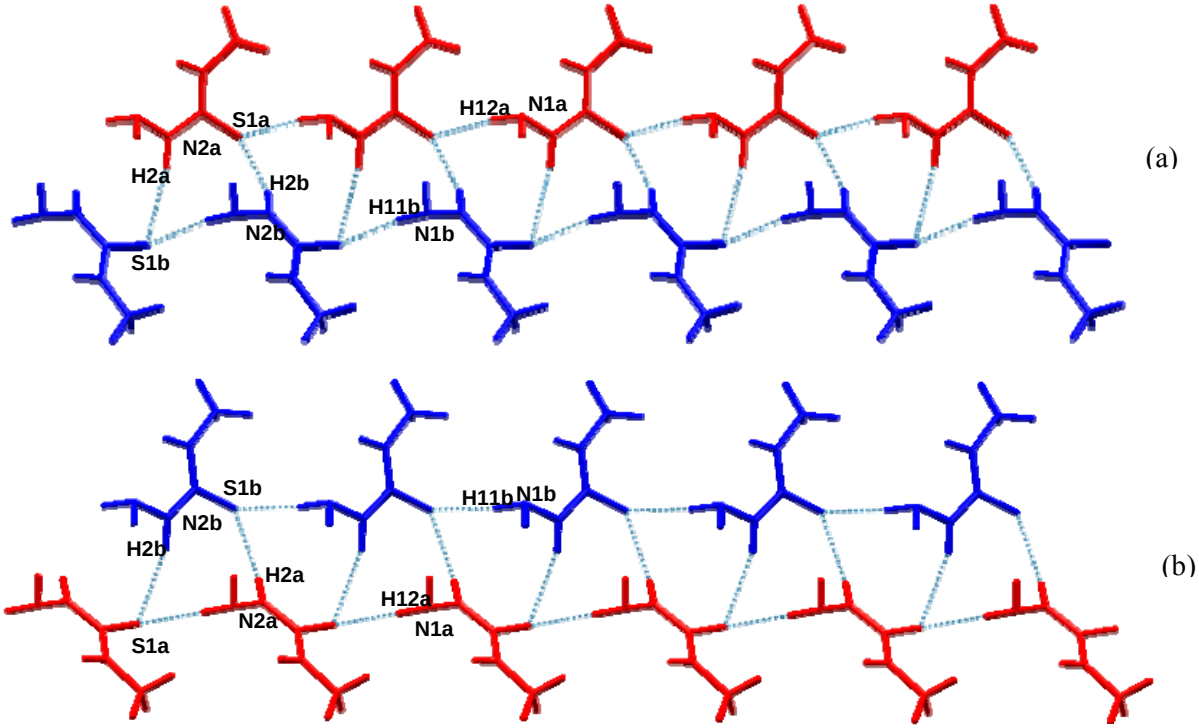

Figure S3. The chains consisting of the same type of molecules (A and B molecules are given in red and blue, respectively), interconnected *via* a pair of the equivalent N2b−H2b···S1a and N2a−H2a···S1b interactions. Two projections of the same fragment, (a) and (b) are given to illustrate very similar geometry and mutual orientation for both of interactions. In order to compare the geometry of the interactions N2b−H2b···S1a and N2a−H2a···S1b the upper chains in both presentations have the same orientation.

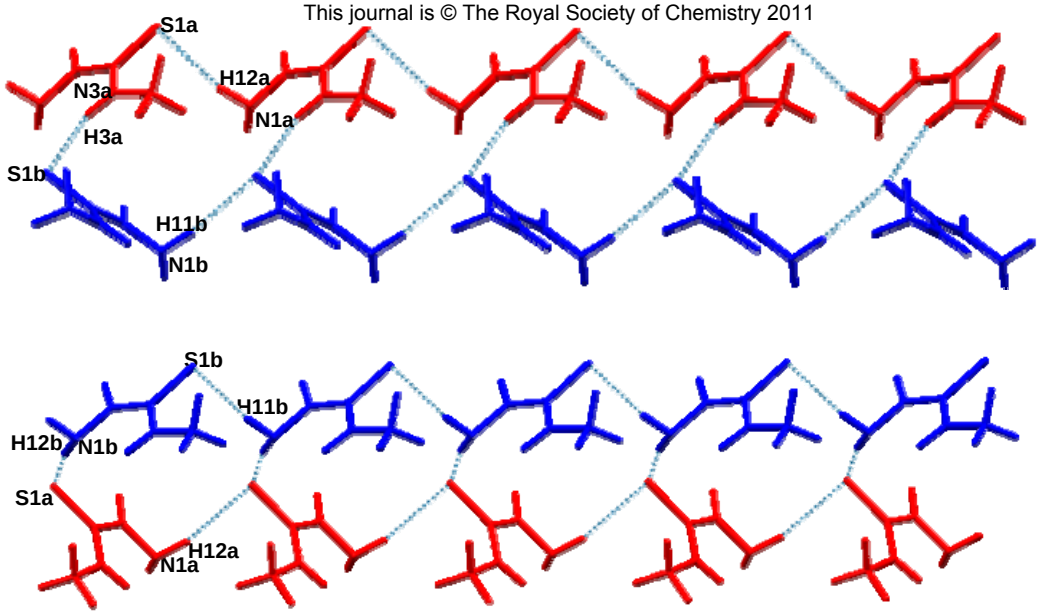

Figure S4 The chains consisting of the same type of molecules (A and B molecules are given in red and blue, respectively) interconnected *via*: (a) N3a−H3a···S1b and (b) N1b−H12b···S1a interactions. In contrast to the interactions presented in Figures 2 and 3 this pair is not equivalent for two acceptors, S1a and S1b. In order to compare the geometry of the interactions N3a−H3a···S1b and N1b−H12b···S1a the upper chains in both presentations have the same orientation.

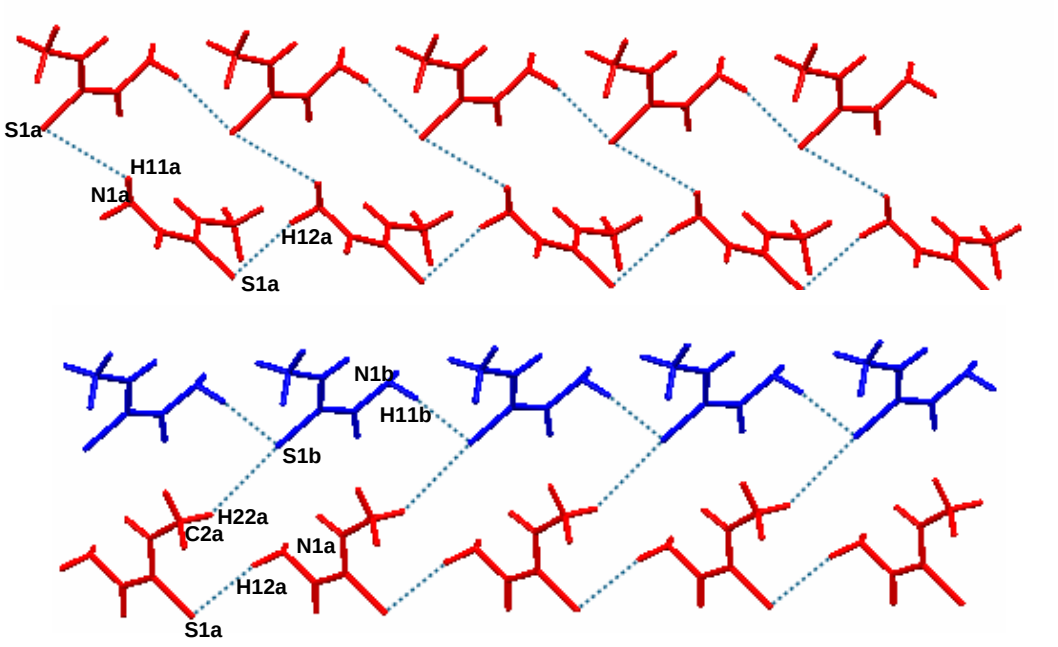

Figure S5. The chains consisting of the same type of molecules (A and B molecules are given in red and blue, respectively) interconnected *via* weak: (a) N1a−H11a···S1a and (b) C2a−H22a···S1b interactions. In contrast to the interactions presented in Figures 2 and 3 this pair is not equivalent for two acceptors, S1a and S1b. In order to compare the geometry of the interactions N1a−H11a···S1a and C2a−H22a···S1b the upper chains in both presentations have the same orientation.

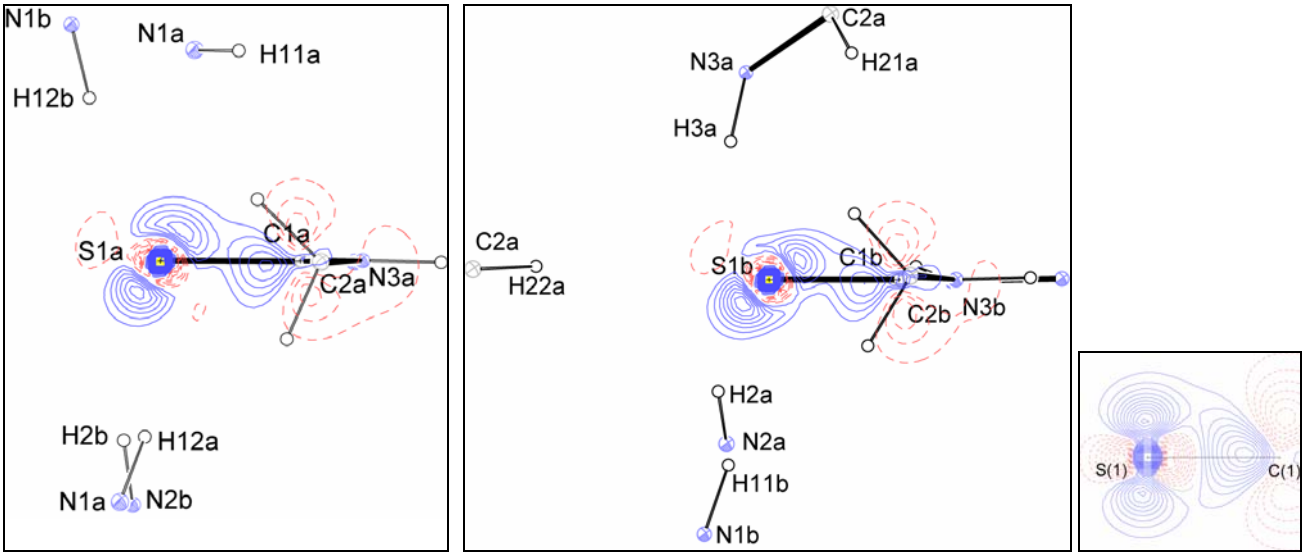

(a) (b) (c)

Figure S6. (a) and (b): Static deformation electron density maps in the planes perpendicular to molecular and containing C−S bond for MeTSC molecules A and B, showing the spatial disposition of H atoms participating in D−H···S interactions. In both cases two equivalent (chemically same donors) and strong interactions are below the molecular plane. (c): Static deformation electron density map for SalTSC in the same plane as for MelTSC. (contours at 0.1 e $Å^{-3}$).

APPENDIX S1: Additional information for experimental charge density analysis of MeTSC and SalTSC.

It is known that description of the valence electron density of the S atom in the experimental charge density analysis could be rather problematic.[1] For two compounds[2,3], where the corresponding S atoms can be considered to have the most similar intramolecular connectivity, as in the present case, the highest concentration of residuals is found in the vicinity of the S atom. In the study[3] of the thioacetamide featuring the two molecules in the asymmetric unit, high residual peaks in the lone pair regions indicated that the electron density could not be successfully modeled for either of the molecules (molecules could not be treated separately). Therefore, presenting average electronic features of the molecules has been the only option. The quality of our results, particularly in relation to the S atoms region, gives us an opportunity to do a quantitative analysis of the electronic features of S atoms and the intermolecular interactions which engage them. The refinement statistics for charge density studies for MeTSC and SalTSC are given in Tables S3 and S4. The residual density maps, covering the resolution range which is considered as the most relevant for diffraction of valence electron density ($\sin\theta/\lambda$ = 0.00 to 0.80 $Å^{-1}$) in the vicinity of the sulfur atoms, show no peaks outside the range –0.07 to 0.12 e $Å^{-3}$ for MeTSC (Figure 2, main text) and –0.07 to 0.08 e $Å^{-3}$ for SalTSC (Figure S9). The residual density maps in a full data range are also practically featureless (Figures S7, S8).

Table S3. Summary of the least-squares refinements for MeTSC.

	Spherical atom model	High Order	Pval-κ model	Multipole model
sinθ/λ range	0.0-1.1	0.8-1.1	0.0-1.1	0.0-1.1
Nobs ($I>3\sigma_I$)	7503	3928	7503	7503
Npar	165	108	49	437
R(F)	2.74 %	3.17 %	2.82 %	1.78 %
R_w(F)	3.14 %	3.20 %	3. %	1.99 %
goodness of fit	1.26	0.92	1.34	0.82

Table S4. Summary of the least-squares refinements for SalTSC.

	Spherical atom model	High Order	Pval-κ model	Multipole model
sinθ/λ range	0.0-1.10	0.8-1.10	0.0-1.10	0.0-1.10
Nobs ($I>3\sigma_I$)	5459	2313	5463	5463
Npar	154	117	45	449
R(F)	3.97 %	4.53 %	3.39 %	2.11 %
R_w(F)	4.65 %	4.43 %	4.31 %	2.29 %
goodness of fit	1.91	1.07	1.77	0.98

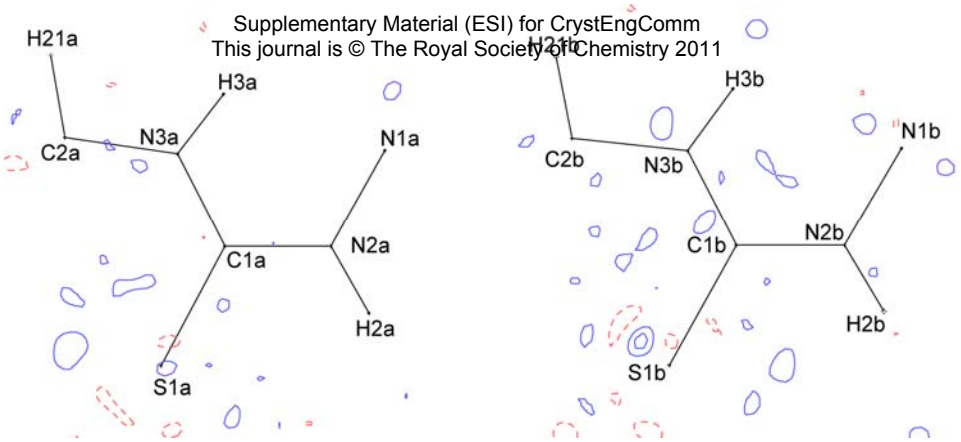

(a) (b)

Figure S7. Residual density maps for MeTSC, molecules A (a) and B (b) in the corresponding C1/N2/N3 planes, in the whole resolution range, $(\sin\theta)/\lambda)_{max}$ = 1.1 Å^{-1}. Positive contours shown with solid blue lines, negative contours with dashed red lines. The contour intervals are at 0.1 e Å^{-3}.

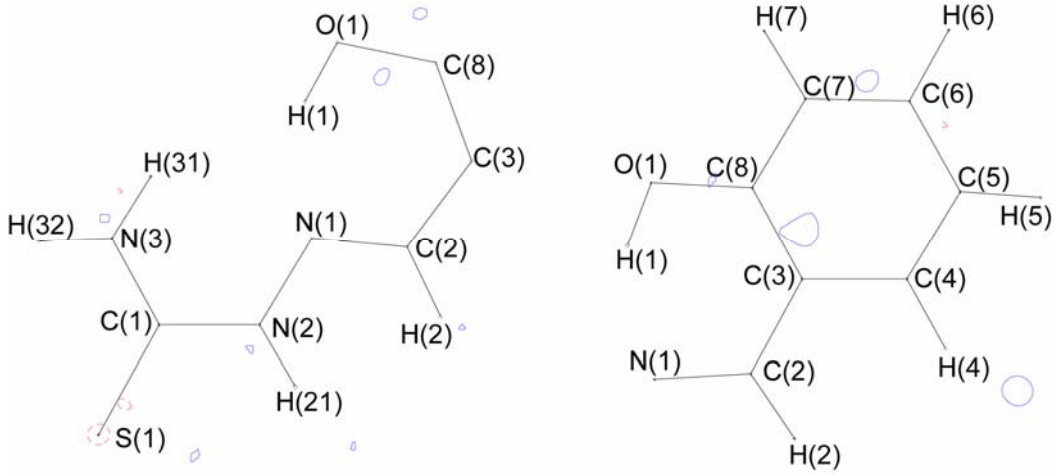

(a) (b)

Figure S8. Residual density maps for SalTSC in (a) C1/N2/N3 and (b) C3/C4/C8 planes, in the whole resolution range, $(\sin\theta)/\lambda)_{max}$ = 1.1 Å^{-1}. The contour intervals as above.

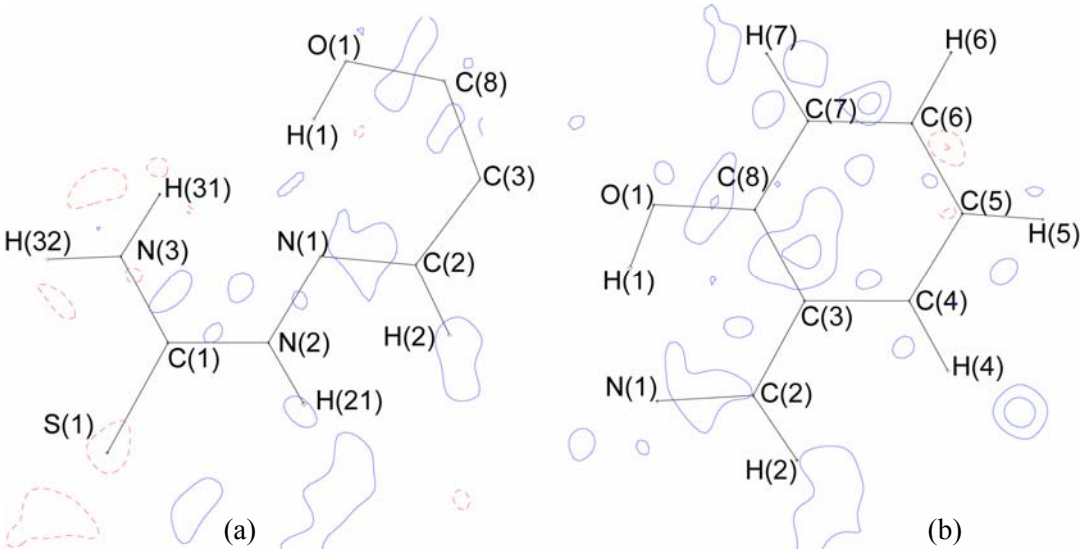

(a) (b)

Figure S9. Residual density maps for SalTSC. (a) and (b) in the C1/N2/N3 and C3/C4/C8 planes, respectively, for $((\sin\theta)/\lambda)_{max}$ = 0.8 Å^{-1}. The contour intervals are at 0.05 e Å^{-3}.

Table S5. Bond lengths (Å) in MeTSC.

Bond	Molecule A	Molecule B
S1−C1	1.7162(4)	1.7067(3)
N1−N2	1.4065(5)	1.4127(5)
N1−H11	1.001(10)	0.994(9)
N1−H12	0.982(9)	0.986(9)
N2−C1	1.3480(5)	1.3475(4)
N2−H2	0.977(10)	0.975(9)
N3−C1	1.3255(4)	1.3321(4)
N3−C2	1.4476(5)	1.4521(5)
N3−H3	0.963(10)	0.963(9)
C2−H21	1.084(12)	1.073(11)
C2−H22	1.045(11)	1.065(11)
C2−H23	1.086(12)	1.076(10)

Table S6. Bond angles (°) in MeTSC.

Bond angles	Molecule A	Molecule B
H11−N1−H12	108.8 (8)	105.2(7)
H11−N1−N2	106.4(5)	109.3(5)
H12−N1−N2	108.0(6)	106.4(5)
N1−N2−C1	119.35(3)	120.49(3)
N1−N2−H2	120.9(5)	117.6(5)
C1−N2−H2	119.8(5)	120.4 (6)
C1−N3−C2	125.32(3)	123.31(3)
C1−N3−H3	115.1 (6)	116.5(5)
C2−N3−H3	119.5(6)	120.1(5)
S1−C1−N2	118.29(3)	119.37(3)
S1−C1−N3	124.59(3)	123.38(3)
N2−C1−N3	117.12(3)	117.24(3)
N3−C2−H21	107.5(6)	107.0(6)
N3−C2−H22	110.0(6)	110.1(6)
N3−C2−H23	109.8(6)	107.7(5)
H21−C2−H22	110.8(9)	118.4(8)
H21−C2−H23	109.8(9)	107.1(8)
H22−C2−H23	109.0(9)	106.0(8)

(1) (a) M. Dominiak, P. Coppens, *Acta Crystallogr. Sect. A*, 2006, **62**, 224-227. (b) E. Espinosa, E. Molins, C. Lecomte, *Phys. Rev. B*, 1997, **56**, 1820-1833.
(2) P. Munshi, T. S. Thakur, T. N. Guru Row, G. R. Desiraju, Acta Crystallogr. *Sect.B*, 2006, **62**, 118-127.
(3) T. W. Hambley, D. E. Hibbs, P. Turner, S. T. Howard and M. B. Hursthouse, *J. Chem. Soc., Perkin Trans. 2*, 2002, 235−239;

APPENDIX S2: Theoretical aspects of the topological analysis and the analysis of the molecular electrostatic potential.

The topological analysis of the total electron density based on Bader's "Quantum Theory of Atoms in Molecules", (QTAIM)[1] has been used to provide quantitative characterization of the chemical bonds and intermolecular interactions. According to this approach, the extrema of the electron density, ρ(r) (minima, maxima or saddle points) are associated with the critical points where the first derivative of the electron density vanishes i.e. $\nabla\rho(r) = 0$. Of particular importance are (3, –1) the bond critical points (BCP's) which are unequivocal indicators of the existence of interatomic interactions. The topological properties at the BCP i.e. values of the charge density (ρ_{bcp}), Laplacians ($\nabla^2\rho_{bcp}$), ellipticities (ε) and the eigenvalues of the Hessan matrix (λ_1, λ_2 and λ_3) can be used to distinguish between various types of interactions. The negative values of the Laplacian, accompanied by high density values at the BCPs, reflect the covalent character of the bonds ("shared-shell interactions"), while positive values in the Laplacian, accompanied by relatively small values of the electron density, are attributed to "closed-shell interactions", such as hydrogen bonds, or ionic interactions.

The topological analysis of the electron density also enables derivation of the local energetic properties. The kinetic energy density at the BCP's G(r), which is considered as proportional to the ionic character of the interatomic interactions, is estimated using the approximation of Abramov[2]:

$$G(r) = \frac{3}{10}(3\pi^2)^{2/3}\rho(r)^{5/3} + (\frac{1}{6})\nabla^2\rho(r)$$

The potential energy density V(r) at the BCPs is related to the bond covalence and it is obtained from the local form of the virial theorem:

$$V(r) = \frac{1}{4}\nabla^2\rho(r) - 2G(r)$$

The sum of the kinetic and potential energy densities represents the total energy density H(r). The negative value H(r) at BCP usually implies that a bond is of a covalent nature.

In addition, the topological analysis of the negative Laplacian ($-\nabla^2\rho_{bcp}$), i.e. a search for (3, –3) critical points, was performed in order to localize and quantify maximum charge concentrations in the bonding and non-bonding regions of the atom valence shell. The peaks of the negative Laplacian are called valence shell charge concentrations (VSCCs).

According to the QTAIM[1], atomic electron density is surrounded by the interatomic surface defined by the zero-flux condition of the gradient field that delimits the atomic basins. Integration of the electron density over the atomic basins results in the corresponding topological atomic charges.

We used the XDPROP and TOPXD programs incorporated in the XD program package[3] to determine the topological properties of the MeTSC molecule.

Electrostatic potential. A very important additional property derived from the experimental electron density distribution is molecular electrostatic potential, U(r)[4]. It is given as a sum of contributions of the positive nuclear charge Z_{at} and the pseudoatom electron density ρ_{at} at R_{at}:

$$U(r) = \sum_{at}^{molecule} \frac{Z_{at}}{r - R_{at}} - \int \frac{\rho_{at}(r')}{|r - R_{at} - r'|} d^3r'$$

Molecular electrostatic potential (MEP) can, by revealing the molecular parts which are more likely to interact, provide the information about how a molecule interacts with its surroundings. The fact that the molecular interaction energy is usually dominated by the electrostatic part, gives enough ground

to use the electrostatic potential as a sensitive tool for prediction of the strength of the intermolecular interactions. MEP was calculated by XDPROP program, while the graphical software MOLEKEL[5] was used for 3D visualization. In addition to the chosen isopotential surfaces, the MEP was also plotted on the molecular isodensity surface of 0.001 au, originally proposed by Bader in his work on molecular surfaces.[6]

(1) R. F. W. Bader, Atoms-in-Molecules: A Quantum Theory,Clarendon, Oxford, 1990.
(2) Y. A. Abramov, *Acta Crystallogr., Sect. A*, 1997, **53**, 264−272.
(3) A. Volkov, P. Macchi, L. J. Farrugia, C. Gatti, P. Mallinson, T. Richter and T. Koritsanszky, XD2006: A Computer Program Package for Multipole Refinement, Topological Analysis of Charge Densities and Evaluation of Intermolecular Energies from Experimental and Theoretical Structure Factors, 2006.
(4) (a) N.−E. Ghermani, N. Bouhmaida and C. Lecomte, *Acta Crystallogr., Sect. A*, 1993, **49**, 781−789; (b) N. Bouhmaida, N.−E. Ghermani, C. Lecomte and A. Thalal, *Acta Crystallogr., Sect. A*, 1997, **53**, 556−563; (c) P. Politzer and D. G. Truhlar, *Chemical Applications of Atomic and Molecular Electrostatic Potentials*, Eds. Plenum, New York, 1981.
(5) S. Portmann and H. P. Lüthi, MOLEKEL: An Interactive Molecular Graphics Tool. *Chimia* 2000, **54**, 766-770.
(6) R. F. W. Bader, M. T. Carroll, J. R. Cheeseman and C. Chang, *J. Am. Chem. Soc*. 1987, **109**, 7968-7979.

APPENDIX S3: Electrostatic potential as a predictive tool for analysis of intermolecular interactions of thioureido S acceptor.

Molecular electrostatic potential (MEP) is a very sensitive physical property which responds to any changes in the electron density distribution of the molecule (and its surroundings). Electrostatic potential shows complementarity between positive regions of H-donors and negative regions of the H-acceptor. That is why MEP is often attributed with capabilities to accurately describe and even predict intermolecular interactions and molecular reactivity. As hydrogen bonds are usually considered essentially electrostatic, studying of MEP should be considered as one of the main tools in researching hydrogen bonds. This is of particular importance in the case of thioureido S acceptor as the ab initio calculations of the total interaction energy of O−H···S and N−H···S interactions[1] have shown that these interactions are mainly electrostatic in nature. The investigation of MEP should also have a prominent role in the analysis of weak, long-range interactions for at least two reasons: a) as in these cases the dominance of the electrostatic character is unambiguous[2]; b) considering that MEP decreases gradually because of 1/r dependence.

The use of MEP for an analysis of intermolecular interactions is particularly valuable when the experimental MEP for a molecule in the crystalline environment is compared to the theoretical MEP, for an isolated molecule. The analysis of changes in shape and magnitude of MEP gives a clear indication about the effects of intermolecular interactions. In accordance with the above mentioned, and taking into account the topic of our research, our interest focused on the negative MEP in the region of S acceptor. In order to make a comparison we also employed quantum mechanical calculation to determine MEP and negative Laplacian of the electron density for a series of the isolated molecules (20 in total) belonging to the same thioureido family.

The tasks were the following:

- compare similarities and differences of the S acceptor in various thioureido compounds (20 molecules in gas-phase), subsection 3.1.
- compare the S thioureido acceptor to the C=O carbonyl acceptor, as the latter is a common acceptor, subsection 3.2.
- examine changes and values of the negative MEP of the S acceptor in different directions against the C−S bond, subsection 3.3.
- examine adaptivity and flexibility of MEP in the vicinity of the S acceptor by comparing the experimental MEP in a crystaline form to the theoretic MEP in gaseous state, subsection 3.4.

3.1. Spatial distribution of the sulfur lone pairs electron density (LPED). Similarities and differences in various thioureido compounds.

Any analysis of the capability of the sulfur atom to serve as an acceptor for hydrogen bonding should take into account spatial distribution of its lone pairs electron density (LPED). The LPED spatial distribution has a decisive effect on any H-acceptor when it comes to spatial and geometrical preferences for hydrogen bonding. In other words, number and spatial directionality of lone pairs (and spatial distribution of their electron density) have a direct effect on hydrogen bonding directionality and capacity of the acceptor to form one or more hydrogen bonds. For instance, carbonyl oxygen acceptor has two lone pairs located in the C−C(=O)−C plane making that particular plane more favourable and preferable in H-bonds formation, while position and directionality of the two lone pairs have effect on the hydrogen-bonding geometry.

Therefore, LPED distribution for S thiureido acceptor is of crucial importance for an analysis of its acceptor capabilities. Our experimental charge density results for MeTSC and SalTSC have already shown that LPED for S is torus-shaped. As these molecules are located in the crystal lattice, their torus is partially deformed under the influence of formed H-bonds and intermolecular interactions. This led us

to employ theoretical calculations and to analyze the torus in several more different tioureido-based compounds in the gaseous state. The topological characterization of the negative Laplacian of electron density ($-\nabla^2\rho(r)$ is an excellent tool for analysis of accumulation of electron density that is typical for the lone pairs. In the case of 19 different tioureido molecules, we have established that their toruses are of similar quality (by shape and symmetry) and quantity (by the Laplacian values in torus and the distribution of these values within the torus itself). Figure S10 shows 2D distribution of Laplacian in 3 characteristic planes. Torus-shaped accumulation in the valence shell of S which corresponds to LPED is quite homogeneously, symmetrically and continuously distributed around the S atom (in relation to the C−S axis). Slightly higher accumulations exist only in the N−C(=S)−N plane (Figure S10c, Projection through a torus). The greatest electron density accumulation forms a circular shape with very similar negative Laplacian values in all 19 thioureido-based molecules. These values are in the range of *cca* 11.8 (in the N−C(=S)−N plane) to *cca* 7.7 e Å^{-5} (in the orthogonal plane). In the acetone's carbonyl O atom, contrary to the S acceptor, accumulations in the N−C(=O)−N plane are over 5 times greater than those in the orthogonal plane. It is also interesting to note that maximum accumulations of all 19 molecules are almost at the same distance of nuclear positions (nucleus of S atom) – 0.69-0.70 Å (0.33 Å for the O atom in acetone).

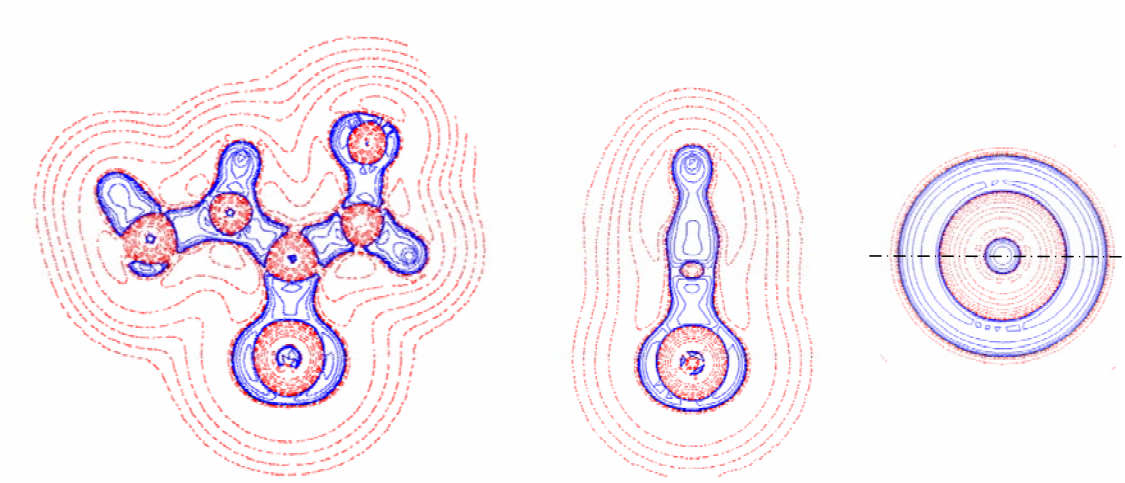

a) b) c)

Figure S10. 2D plot of the theoretical Laplacian of S1 in MeTSC (molecule A) in three orthogonal planes: (a) molecular plane; (b) normal to the molecular plane, containing the C=S bond; (c) normal to the molecular plane (projection through a torus); Accumulation and depletion of density are given in blue solid and red dashed lines. Contours at $2^m\times10^n$ e Å^{-5}, where m = 1, 2, 3 and n = –3, –2, –1, 1, 2, 3.

LPED distribution for the S thiureido acceptor could also be analyzed using MEP, because (even small) changes in LPED are reflected in the distribution and value of negative MEP. For all 19 molecules in gaseous state, the strong negative electrostatic potential (of –0.060 au) displays very similar shape and spatial distribution (Figure S11, first column) that are in accordance with the toroidal distribution of LPED. When it comes to the values of the negative MEP (Figure S11, 2nd and 3rd column) that extend to the region where H-bonds and intermolecular interactions are formed, the 19 analyzed molecules are also very similar among them. Negative MEP on the S acceptor is very similar in values and in the spatial distribution for all thiouredo compounds regardless of significant structural differences among the substituents at nitrogen atoms from N−C(=S)−N tiouredo fragments (substituents H_2, $-CH_3$, −N−ciclopentane, CH_2−Ph, −N−C(CH_3), −Thiophene, −Pyridine, −C(NH_2)$_2$, −N−indole, −N−CH−pyrrole).

An explanation of torus similarities in all 19 molecules can be the fact that the first- and second-neighboring atoms (C and N respectively) for the S acceptor are always the same atoms, so that structural variations in the substituents, (taking into consideration that they are the third-order neighborhood for the S acceptor) do not have an important impact on electronic characteristics of the S acceptor which is a terminal atom in the thioureido fragment. These similarities of the different thioureido S acceptors (and also the above described similarities in the Laplacian distribution and values) are significant because it means that the experimental results for MeTSC and SalTSC in this work, as well as the further analysis applied during the MeTSC testing in the gaseous phase, can be applied to the S atom in tioureido-based compounds in general.

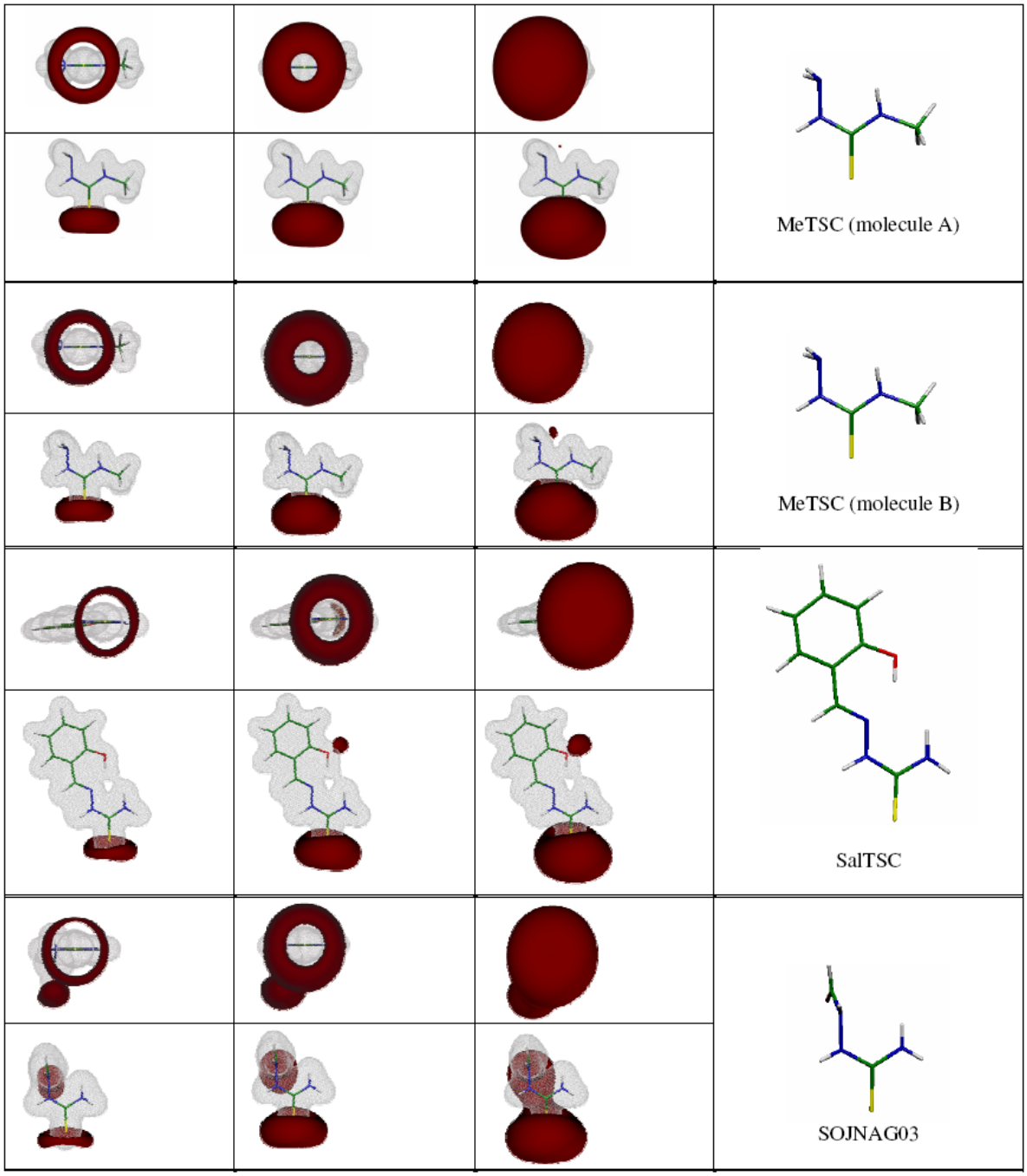

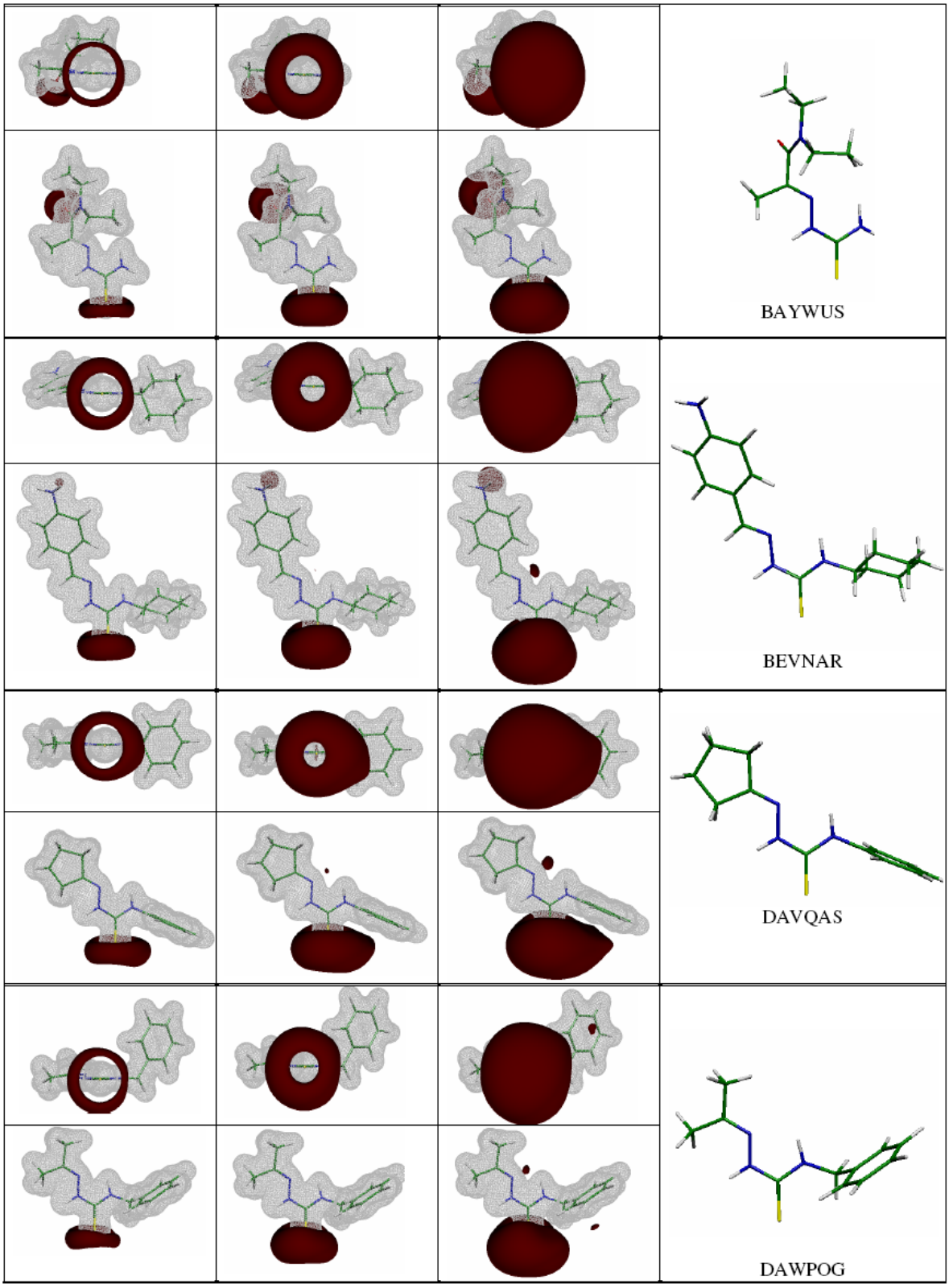

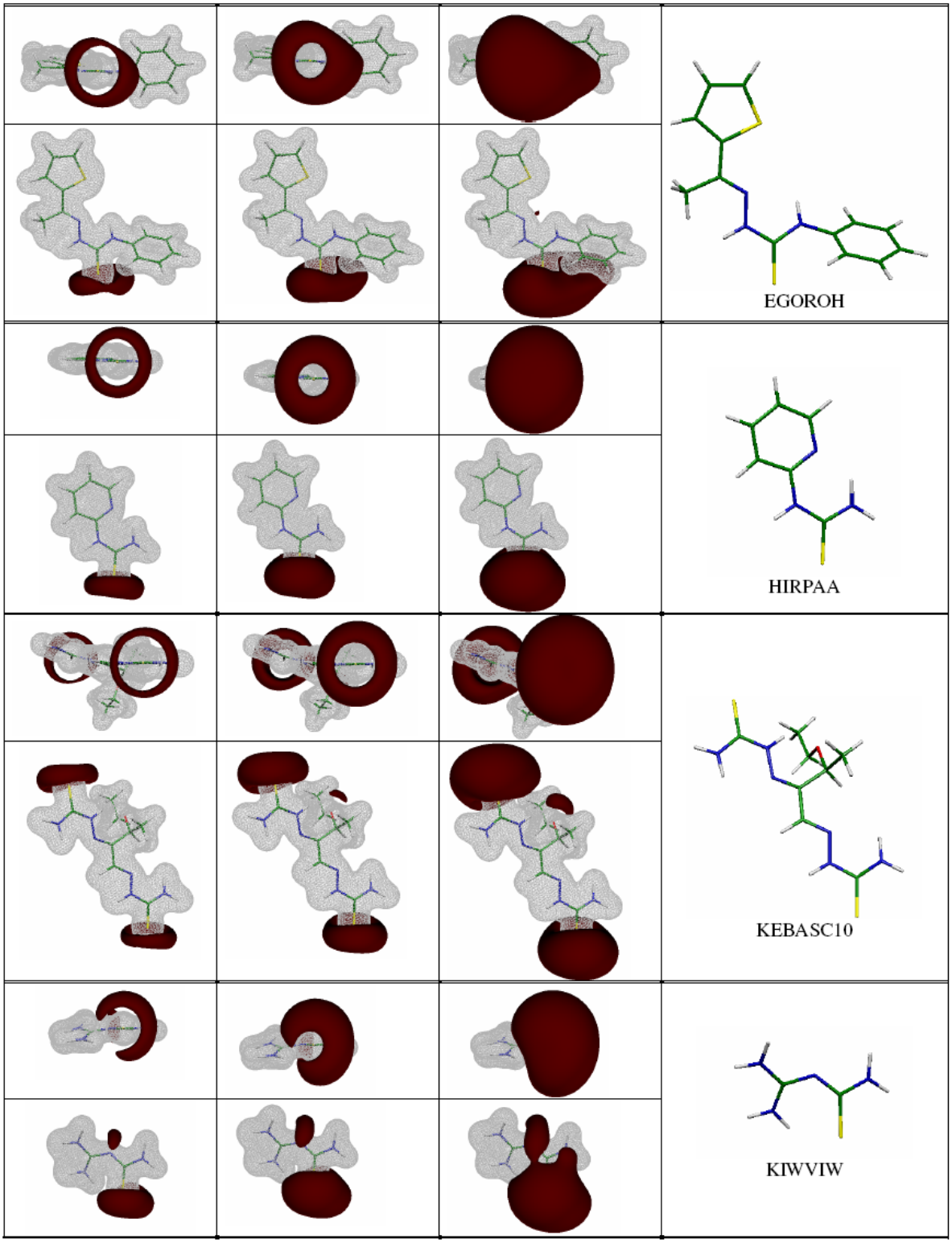

			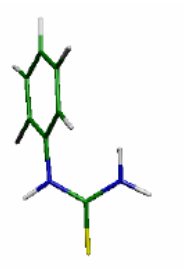 NUTPAT
			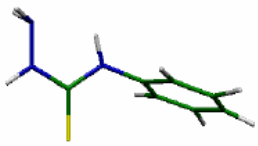 PHTSEM
			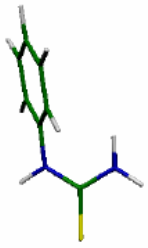 QQQDDM01
			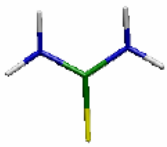 THIOUR14

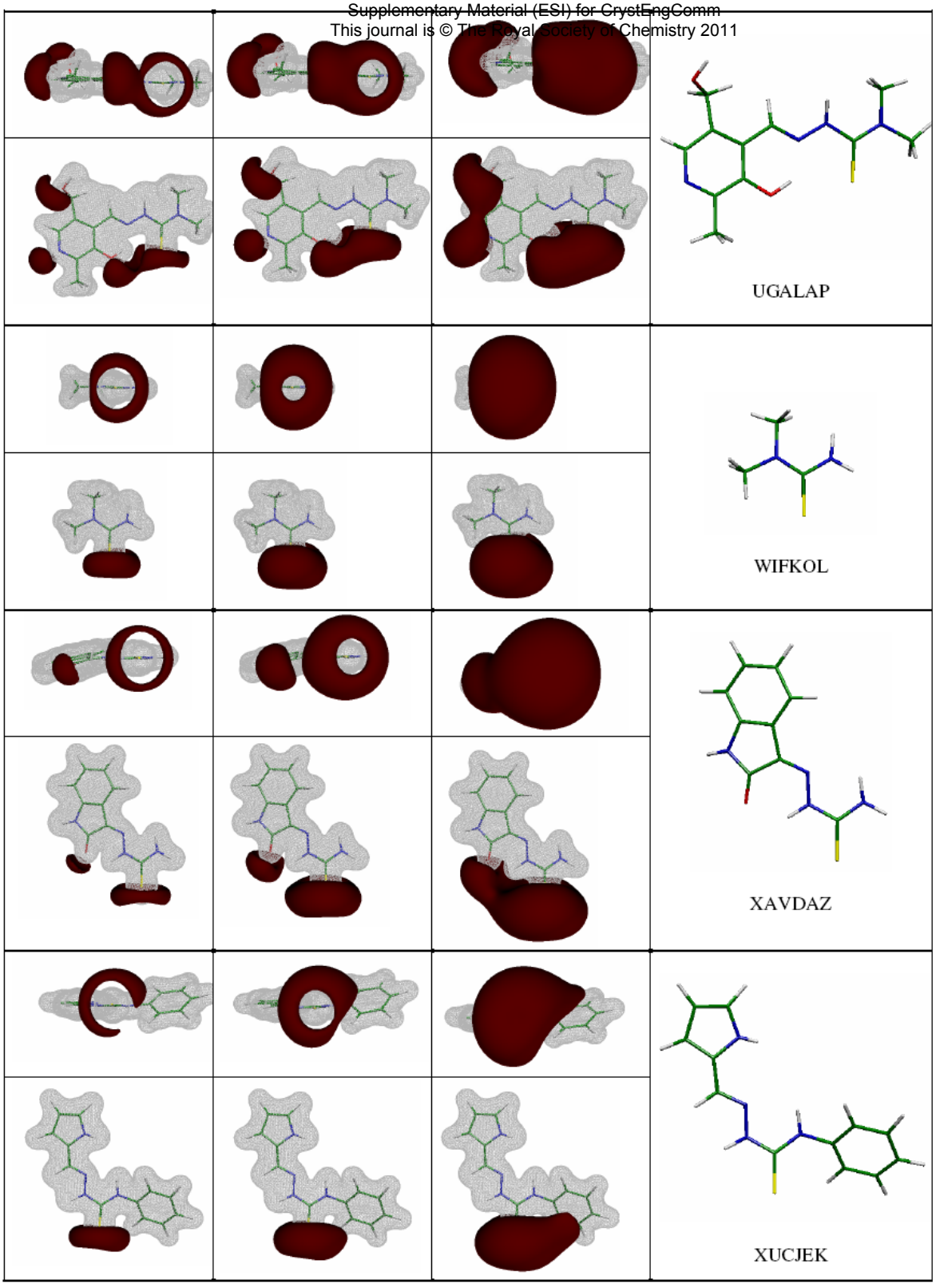

Figure S11. Distribution of MEP for the different thioureido based molecules placed in the gas phase (results of the theoretical calculations), indicating the predominantly toroidal shape and similarity in distribution and magnitude of the negative MEP of S atoms. Red surfaces correspond to the negative MEP's at: −0.060, −0.045, −0.030 au, from left to right, respectively. Gray surfaces correspond to the positive MEP's +0.1 au. Except for the first three molecules which are part our experimental study, the coordinates for the rest of the molecules examined are extracted from the CSD.[6] The molecules are assigned by their CSD refcodes.

3.2. Spatial preferences of the S acceptor in hydrogen bond formation. Comparison to the typical, carbonyl O acceptor.

Toroidal distribution of sulfur's LPED (Figure S10) and consequent distribution of negative MEP (Figure S11) have strong influence to spatial preferences of hydrogen bonds formation. The whole space around the S acceptor (symmetrically around the C−S axis) is almost equally convenient for building of H bonds unlike the carbonyl O acceptor whose two lone pairs are situated in the C−C(=O)−C plane that, as a result, represents a preferred plane for H-bonds. This obvious advantage of the thioureido S acceptor over the carbonyl O acceptor requires more detailed comparison of the electrostatic properties of these two acceptors.

As the oxygen atoms in analogue ureido compounds (due to resonance effects) represent exceptionally good acceptors[1,3], a direct comparison of the thioureido sulfur and ureido oxygen acceptor abilities is, therefore, inappropriate. The situation changes when we consider the carbonyl oxygen from the acetone moiety which is also accepted as a conventional hydrogen bonding acceptor. Figure 7 in the main text compares the spatial distribution (extent and shape) of the theoretically calculated MEP of the thioureido sulfur and the acetone oxygen. In order to make a relevant comparison, we have superponed the molecule skeletons of the MeTSC and acetone, overlapping the positions of S and O atoms and corresponding C−X bonds (X = S and O). The negative isopotential surfaces of both molecules show the same percentage (80 % and 40 %) of the calculated MEP minima. In the case of the O atom the most negative MEP is located in C−C(=O)−C plane, indicating that the highest concentration of LPED remains in the molecular plane (Figure 7, left). The preferable region of influence of the oxygen acceptor and formation of hydrogen bonds can therefore be linearly approximated to the in-plane arc positioned in front of the oxygen. This conclusion is in accordance with the Isostar plots from a CSD study by Wood *et al.*[3] of the spatial distribution of O−H and N−H donor groups around the (urea) O acceptor. The preferable (toroidal) region of influence of the sulfur acceptor can be linearly approximated to the circle drawn around the S atom, indicating that it is equally possible for H-donor to approach the S atom from all potential directions that emerge from a toroidal shape irrespectively of the molecular plane. The interacting area available for stronger hydrogen bonding is obviously larger in the case of sulfur than in the case of oxygen (the sulfur's circle is about 3 times longer than the oxygen's in-plane arc).

For MEP values that stand at 40% of minima the negative MEP surface in both cases expands through space, assuming a hemispheric shape (Figure 7, right). The hemisphere of the voluminous S atom is, however, much larger and reaches farther into space than that of the oxygen atom. Namely, if MEP surface is approximated to the (regular) hemisphere, the sulfur's volume is 2 times larger than oxygen's while the surface is some 1.5 times as large. This larger surface allows the S atom to accept 1.5 times more H atoms due to purely geometrical reasons. These observations suggest that S atom has a much wider interacting area and, consequently, higher hydrogen bonding capacity than the carbonyl O atom.

3.3. Distribution of negative electrostatic potential in different directions in relation to the C−S (C−O) bond

We can analyse MEP values and changes of the tioureido S acceptor in three specific directions:
i) along the C−S bond (in the following discussion labeled as direction D1);
ii) in the direction that forms a 120° angle to the C−S bond and is located in the N−C(=S)−N plane (direction D2);
iii) in the direction that forms a 120° angle to the C−S bond, but is located in the plane orthogonal to the N−C(=S)−N plane (direction D3).

At the same distance from the nucleus of the acceptor (ranging from 2.0 to 3.5 Å), the sulfur has significantly stronger negative MEP than the carbonyl O acceptor from the acetone in all directions except along the C−S bond (Table S7, Figure S12). Since S is a more voluminous atom, such comparison of those two acceptors is biased, (because it gives an advantage to the S acceptor). If we define the area of the molecule for MeTSC and acetone with the isodensity surface of 0.001 au (which is

an accepted criterion for molecular surface[4]), we can establish that the nucleus of the sulfur is more distant from the molecular surface than the nucleus of the oxygen in the acetone by 0.5 Å (i.e. van der Waalls radius for thioureido S is about 0.5 Å longer than the one for O). Therefore, it would be adequate to compare MEP values in the distance range of 2.0-3.5 Å for S to the distance range of 1.5-3.0 Å for O.

Since MEP has a dominating contribution for the long-range directions (i.e. for the longer distances between the acceptor and the H atom), we will analyze the values of negative MEP in the three above-mentioned directions (D1, D2, D3) in the range from 2.5 to 3.5 Å for the thioureido S acceptor and in the equivalent range from 2.0 do 3.0 Å for the O acceptor. The two acceptors show very different distribution of MEP (Table S7). The strongest negative MEP for the O acceptor goes along the extension of the C−O bond (along D1) while the strongest negative potential for the S acceptor goes along the direction D3 (i.e. in the plane orthogonal to the thioureido fragment) which is in accordance with the LPED's toroidal shape. The S acceptor shows stronger negative MEP than the carbonyl oxygen in the whole 1 Å range in all directions except in the D1 (the space of the extension of the C−O/C−S bond). However, in all directions, even in the D1 (the only direction where the O acceptor shows stronger negative potential), the S acceptor shows significantly slower decrease of MEP potential than the O acceptor (Figure S12). In the D1 direction, the negative MEP for O, at a distance of 3.0 Å, decreases by approximately 47% in relation to the value recorded for a distance of 2.0 Å. On the other hand, MEP value for S (in the same direction), at a distance of 3.5 Å, decreases by only 26.4% in relation to the value recorded for a distance of 2.5 Å. In other words, MEP values, recorded initially at distances of 2.0 and 2.5 Å, for both O and S, drop, following an increase in distance by 1 Å, leaving negative MEP for O noticeably weaker than that for S.

Table S7. The decrease of the negative MEP (au) with the distance from S and O acceptors (Å) in different directions.

Distance from the acceptor	D1		D2		D3	
	S	O	S	O	S	O
2.0	-	0.0572	0.0706	0.0502	0.0693	0.0449
2.1	-	0.0535	0.0672	0.0451	0.0666	0.0417
2.2	-	0.0494	0.0636	0.0417	0.0637	0.0382
2.3	0.0394	0.0464	0.0594	0.0380	0.0608	0.0352
2.4	0.0390	0.0434	0.0558	0.0349	0.0574	0.0329
2.5	0.0383	0.0409	0.0522	0.0318	0.0543	0.0306
2.6	0.0375	0.0382	0.0487	0.0295	0.0513	0.0287
2.7	0.0366	0.0362	0.0456	0.0271	0.0484	0.0268
2.8	0.0355	0.0341	0.0425	0.0253	0.0458	0.0247
2.9	0.0345	0.0322	0.0396	0.0237	0.0432	0.0233
3.0	0.0334	0.0305	0.0371	0.0218	0.0409	0.0218
3.1	0.0324	0.0288	0.0348	0.0202	0.0386	0.0205
3.2	0.0313	0.0272	0.0326	0.0188	0.0364	0.0193
3.3	0.0302	0.0259	0.0308	0.0177	0.0346	0.0182
3.4	0.0292	0.0246	0.0289	0.0167	0.0328	0.0172
3.5	0.0282	0.0235	0.0272	0.0156	0.0311	0.0163

At a distance of 2.60 Å (accepted as a short enough distance of O···H in C−H···O hydrogen bonds[5]) in the D2 direction (at the location of the lone pairs for carbonyl oxygen) the O acceptor shows negative MEP (–0.0295 au) that is somewhat weaker than the value of potential for the S acceptor that is at a distance of 3.30 Å in the direction D2 and even 3.50 Å in the direction D3 (Table S7). In other words, the O acceptor in the direction of distribution of its lone pairs, at a distance of 2.6 Å, generates

weaker (or approximately similar) MEP than the S acceptor at distances ranging from 3.3 to 3.5 Å. In the crystal structures of MeTSC and Sal1SC we have found bond critical points for several C−H···S intermolecular interactions with H···S distance of *cca*. 3.1 Å. At this distance, the S acceptor's MEP measures −0.0386 au (Table S7), a MEP value which the O acceptor approximately reaches at distances of 2.20 Å (direction D3), 2.30 Å (direction D2), 2.60 Å (direction D1). Since the C−H···O interactions with H···O at distances of 2.2 to 2.6 Å are declared as hydrogen bonds[5], analogically, the C−H···S interactions with H···S at a distance of 3.1 Å (even up to 3.3-3.5 Å, as shown above) could be accepted as hydrogen bonds.

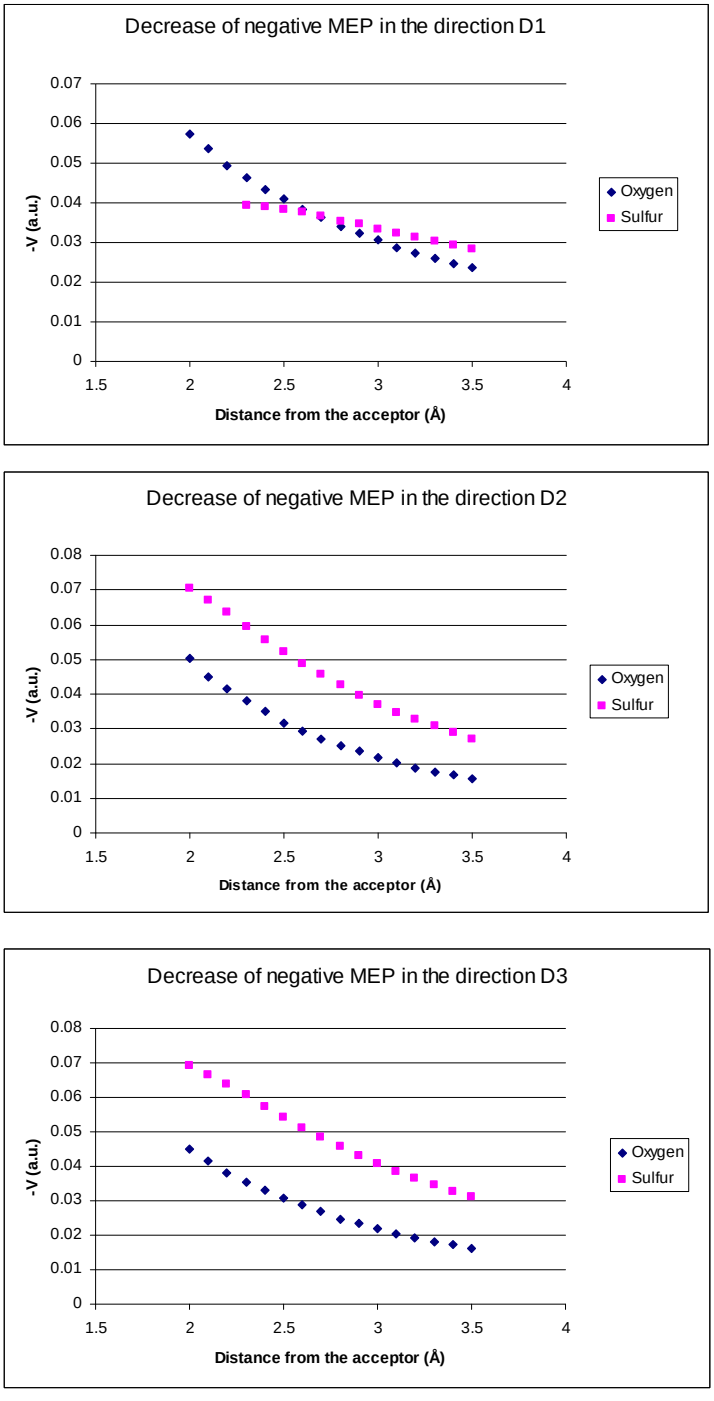

Figure S12. The decrease of negative MEP (au) with the distance from S and O acceptors (Å) in different directions.

Distribution of negative MEP (–0.060 and –0.030 au) against the isodensity molecular surface (0.001 au) for MeTSC, and several other molecules with various O acceptors, is illustrated in Figure S13. When the potential measures –0.060 au (Figure S13, 1st column) it is clear, based on the size and location of the isopotential surface in relation to the molecular surface, that negative potential of the S acceptor even at this shorter distance is somewhat stronger or similar to all other O acceptors, except for the urea.[3a] When the potential measures –0.030 au (Figure S13, 2nd column), the isopotential surface is distributed in the area of weak C−H···O interactions, but in the case of the thioureido S acceptor it occupies a fairly greater space even in comparison to the ureido oxygen, which is a very strong acceptor.

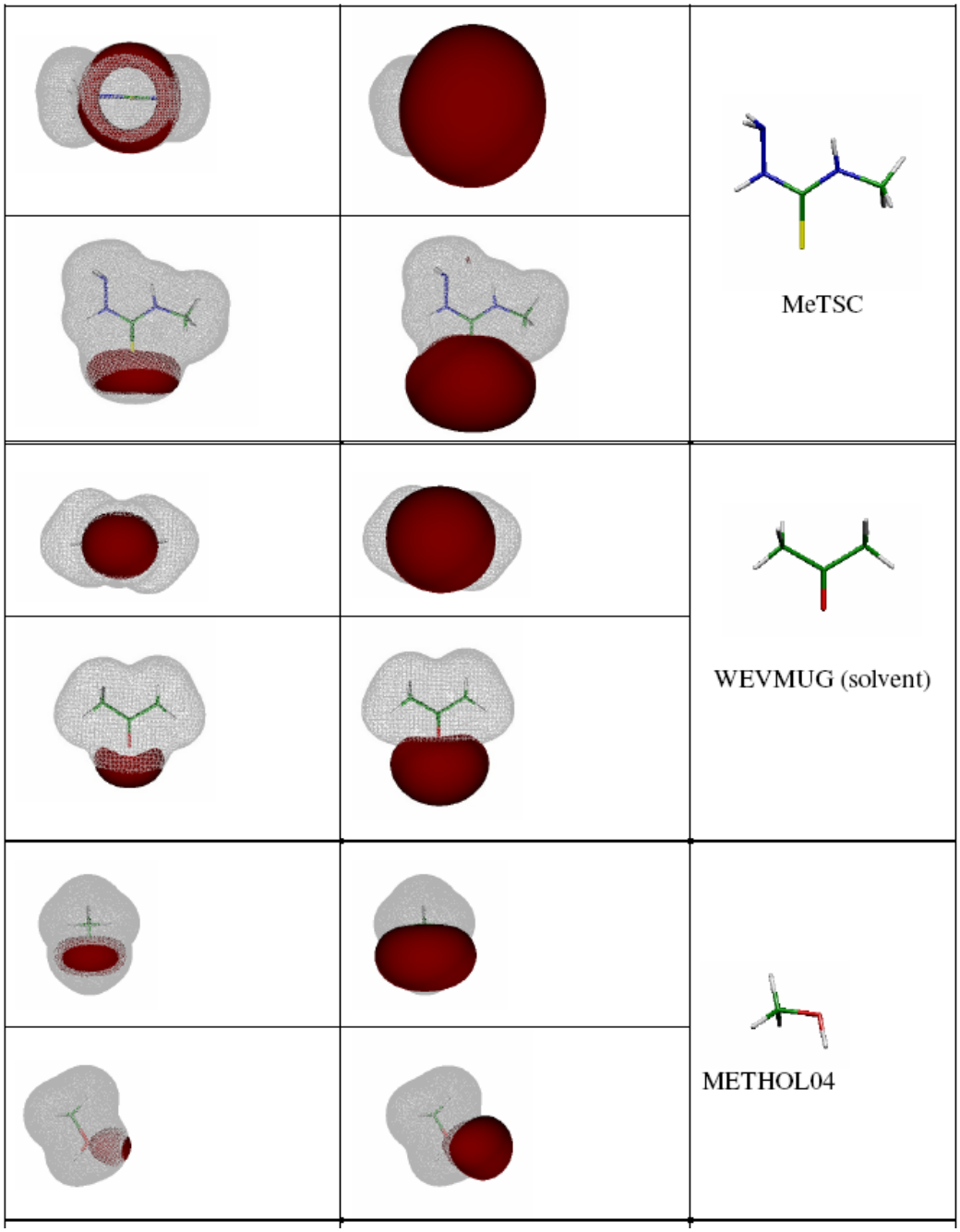

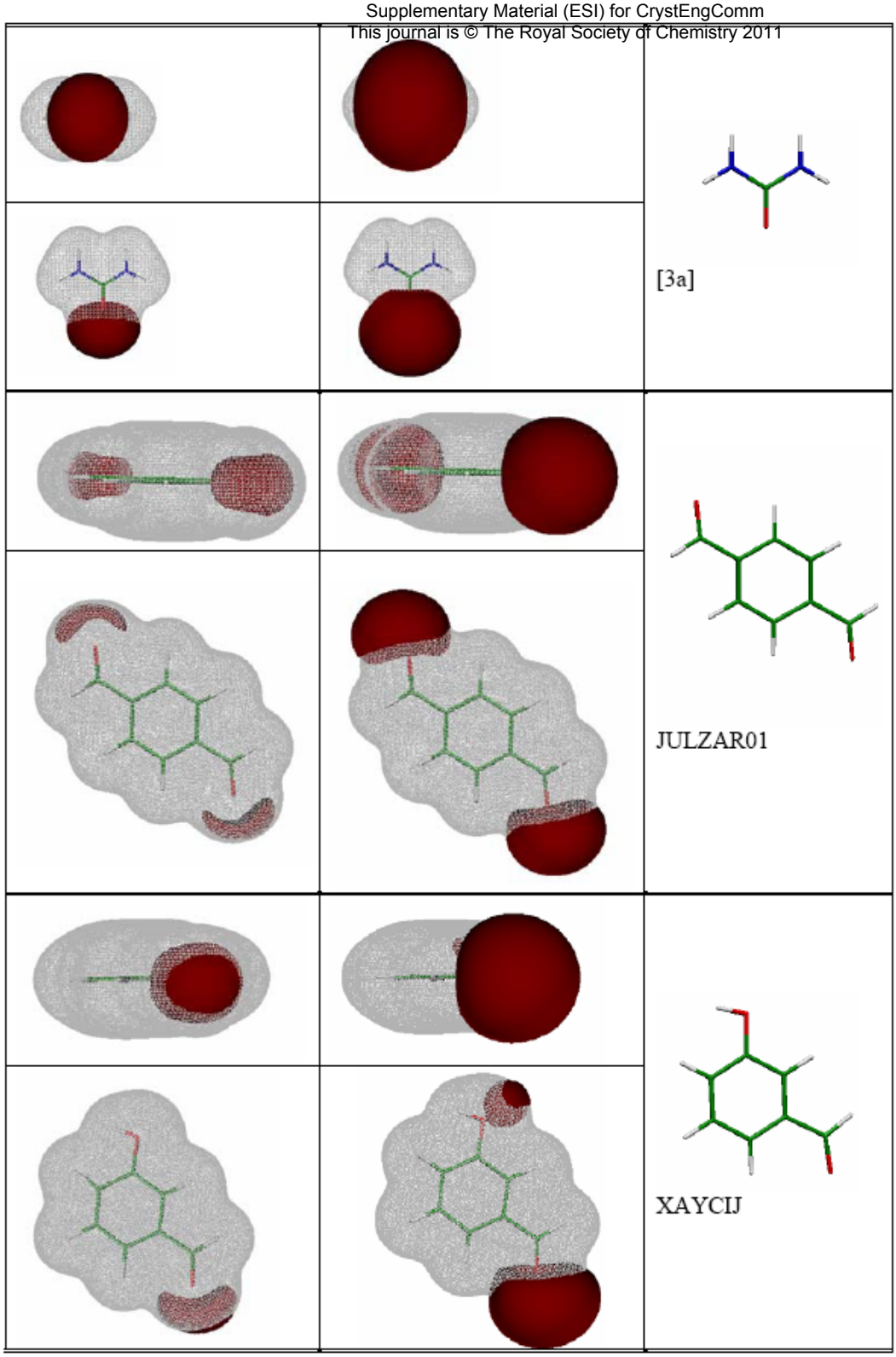

Figure S13. Distribution of MEP at the values of –0.060 and –0.030 au (red surface) with respect to van der Waals's surfaces (ρ(r) = 0.001 au) for MeTSC and different oxygen-containing molecules placed in the gas phase (results of the theoretical calculations). The coordinates for the oxygen-containing molecules are extracted from the CSD.[6] The molecules are assigned by their CSD refcodes.

The isopotental surface for S, measuring (–0.030) au, is more distant, in all directions, from the molecular area boundary (isodensity surface of 0.001 au) than in the case of O from acetone (Figure S14). This difference in distance ranges from almost 0.1 Å along the direction D1, to 0.5 Å along the D3 direction. Illustrated differently, the isopotental surface of the thioureido S acceptor, measuring –0.030, is distant from the acceptor's nucleus from *cca*. 3.36 Å (directions D1 and D2) to 3.58 Å (direction D3), while in the case of oxygen, the corresponding distance is from *cca*. 2.55 Å (direction D2 and D3) to 3.05 Å (direction D1), Figure S14.

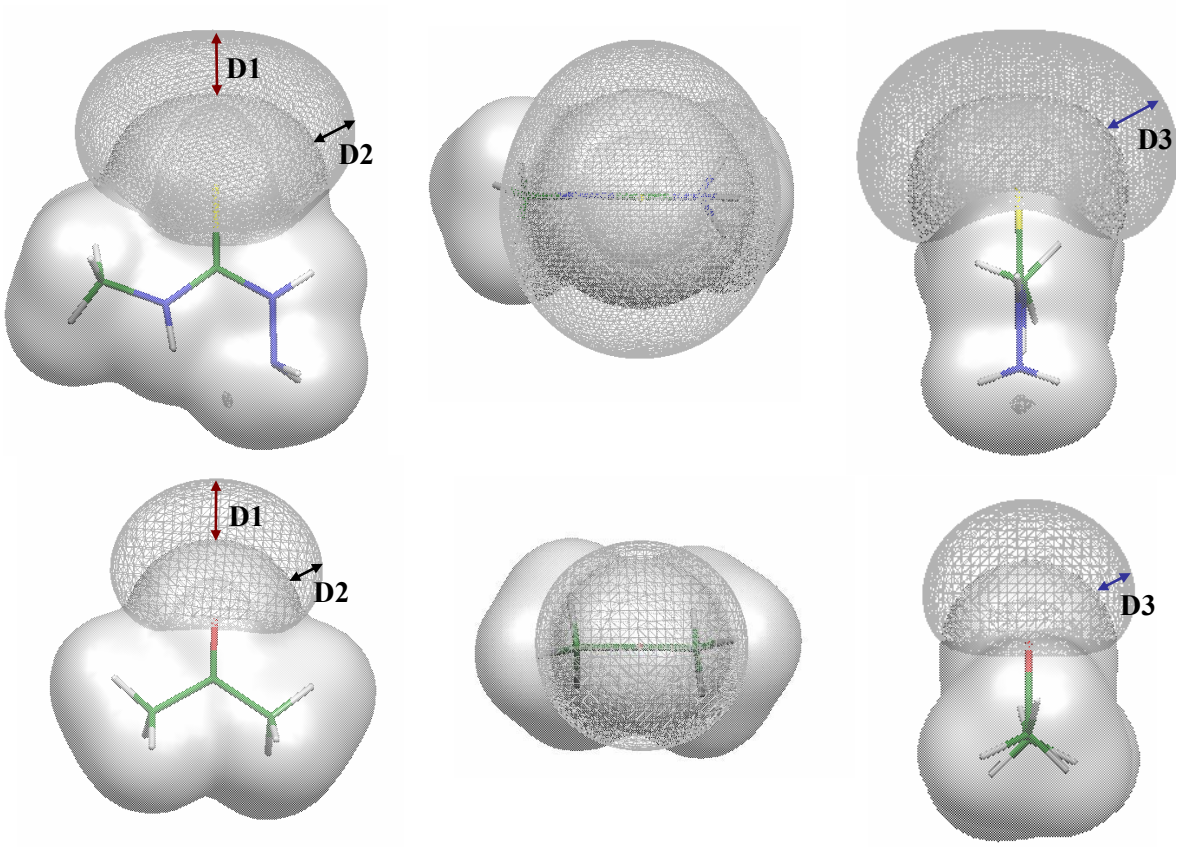

Figure S14. A comparison of the extent of MEP at –0.030 au (grey, chicken) above van der Waals's surfaces (solid, grey) of MeTSC (first row), Acetone (second row). Three orthogonal projections.

Based on the above analysis of the distribution of negative electrostatic potential in different directions, the following can be observed:

- The S acceptor has a very different distribution of its strongest values of negative MEP when compared to oxygen (the strongest negative MEP for S is in the direction D3, while for O it is in the direction D1) and that distribution is in accordance with the toroidal shape of LPED (because of the existance of torus, S shows the strongest MEP along the direction D3).
- The S acceptor has similar or stronger negative potential than the carbonyl O acceptor throughout the whole space except along the C−O bond (D1 direction).
- Negative MEP for S decreases at a significantly slower rate with the distance (in all directions) than it is the case with O. That means that S is a more suitable H acceptor for long-range interactions than oxygen.
- Even in the long H···S distances of 3.3-3.5 Å the thioureido sulfur shows stronger MEP than carbonyl O for distances of 2.6 Å in the direction of dispersion of oxygen lone pairs.
- An area in which the S acceptor reacts with still important MEP of –0.03 au is significantly larger, and it enables storing of a great number of H atoms in the acceptor's neighborhood. This shows that S acceptor, to say the least, is not (except possibly in the direction of C−S bond, direction D1) an inferior H acceptor to oxygen.

3.4. Experimental MEP, distribution and flexibility

As a delicate physical property, experimental MEP changes under the influence of the intermolecular interactions. Therefore, it is interesting to compare distribution of experimental electrostatic potential with distribution of MEP for thioureido-based molecules which are placed in the gas-phase leaving the valence electron densities of the corresponding S atoms unaffected by hydrogen bonds.

Figure S15 displays three-dimensional isodensity surface (0.001 au) of the MeTSC and SalTSC colored in accordance with the experimental MEPs. The region with the most negative electrostatic potential in MeTSC is located on the S atom as was the case with SalTSC. This clearly suggests that these sulfur atoms are relevant acceptors of the intermolecular interactions.

Figure S16 gives isopotential surfaces representation for the same molecules. In the cases of MeTSC and SalTSC, MEP around the S atom, derived from experimental charge density distribution and extracted from the crystalline environment, extremely differs from that observed in the gas-phase (Figure S11) which is almost a perfect torus. The negative surface (of the experimental MEP) distribution in Figure S16 for MeTSC coincides with the side of the acceptors engaged in two strong N−H···S interactions located below the molecular plane (Figure 5, main text), representing sulfur's flexible reaction to the special location of two N−H donor groups. However, SalTSC negative MEP manages to preserve a symmetrical distribution (in relation to the C−S axis) in much the same way as theoretical MEP. This nearly intact distribution can be explained by presence of six D−H donor groups that are almost evenly distributed around the sulfur.

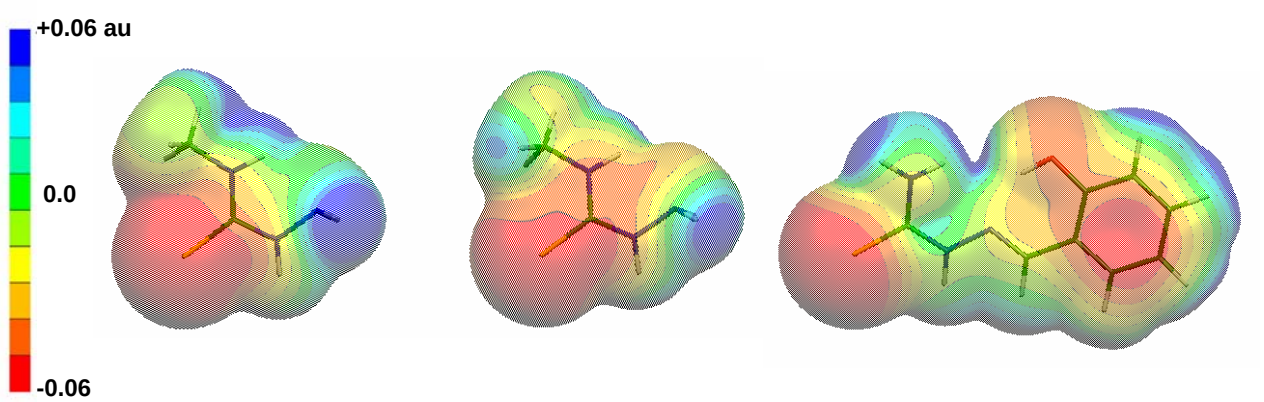

(a) (b) (c)

Figure S15. Molecular electrostatic potential mapped onto 0.001 au isodensity surfaces for MeTSC molecules A (a) and B (b) and SalTSC molecule (c) showing that the region with the most negative electrostatic potential is located in the vicinity of S atoms.

As S adjusts its LPED (in both crystal structures, MeTSC and SalTSC, and for all three molecules) in order to adapt to the environment, it consequently changes the properties of MEP adjusting MEP distribution towards the location of the surrounding H atoms. The experimental MEP, hence, also reflects the flexibility of the S atom.

The analysis of MEP plays a very important role for weak interactions, such as C−H···S. The Figure S17 shows that, in addition to the classical N−H donors, the S atom negative MEP surface in SalTSC is also directed towards the C−H groups. Generally, the S acceptors in tiouredo group show: i) high values of experimental negative MEP and ii) adaptability in distribution of negative MEP towards the spatial arrangement of donor groups (D−H), especially of those with stronger positive MEP.

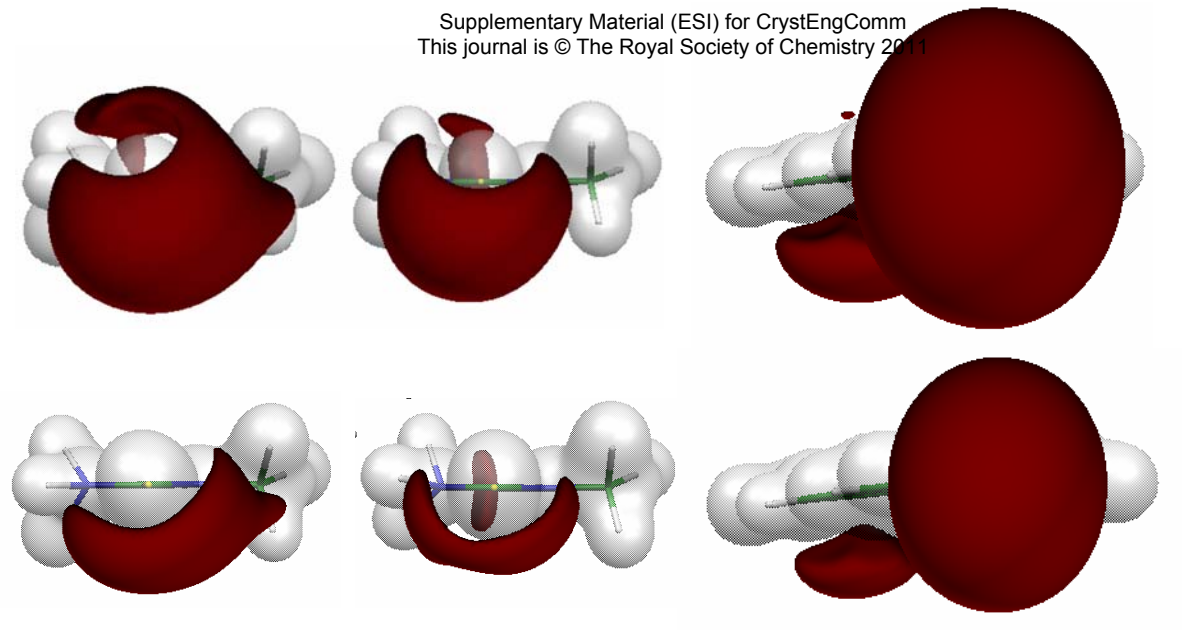

Figure S16. Isosurfaces of molecular electrostatic potential for A, B and SalTSC: +0.100 au (gray), –0.040 au first row, and –0.060 au second row (solid red) as viewed perpendicular on the C−S bond and the molecular plane.

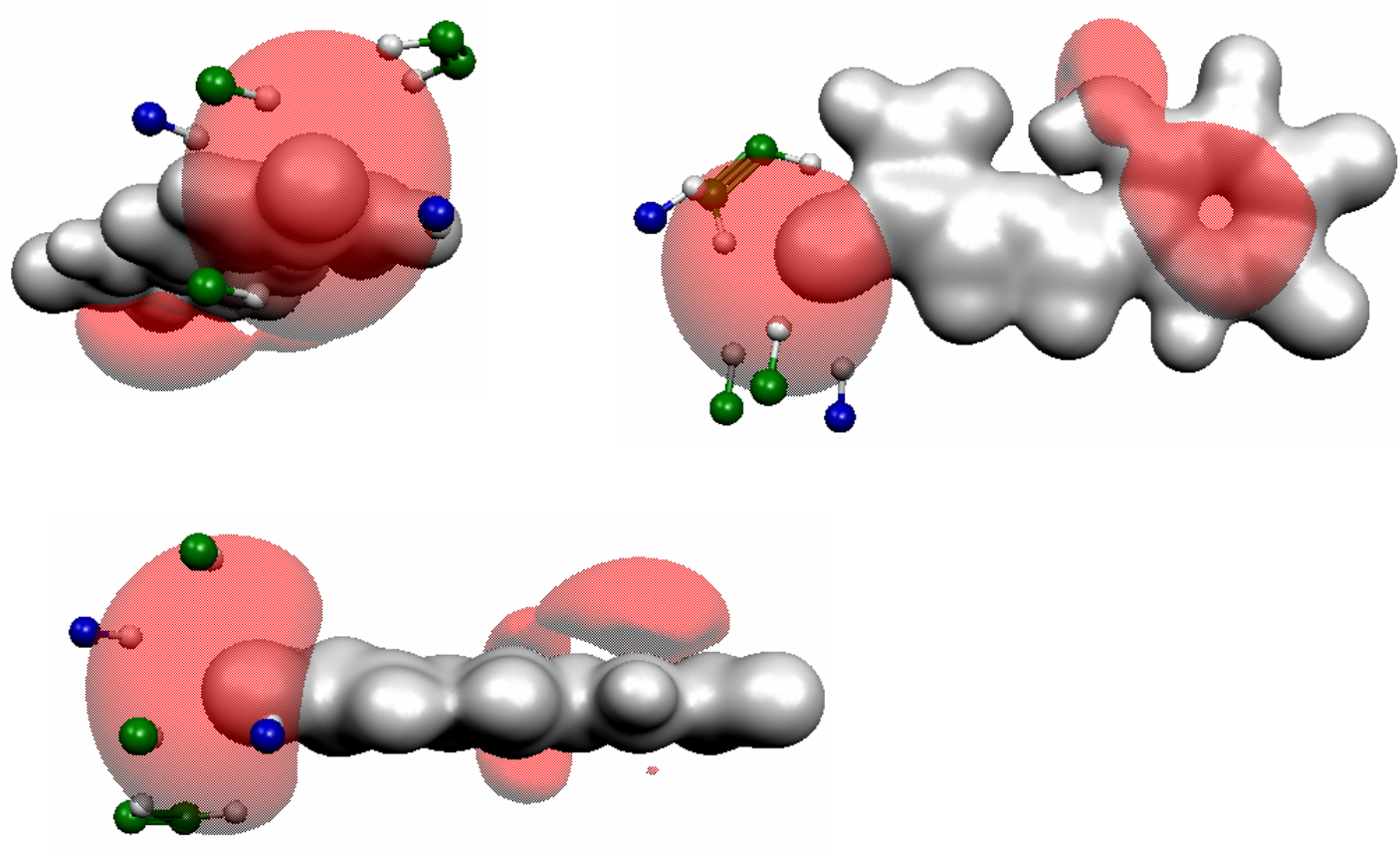

Figure S17. Molecular electrostatic potential isosurface of –0.040 au of the sulfur acceptor directed toward the all surrounding N−H (blue) and C−H (green) donor groups (all six N−H···S and C−H···S interactions are confirmed by the bond critical points in the topological analysis).

(1) P. A. Wood, E. Pidcock and F. H. Allen, *Acta Crystallogr. Sect. B*, 2008, **64**, 491−496.
(2) (a) G. Gilli and P. J. Gilli, *Mol. Struct*. 2000, **552**, 1-15.; (b) A. S. Özen, F. De Proft, V. Aviyente and P. Geerlings, *J. Phys. Chem. A*, 2006, **110**, 5860-5868.
(3) (a) H. Birkedal, D. Madsen, R. H. Mathiesen, K. Knudsen, H. P. Weber, P. Pattisond and D. Schwarzenbach, *Acta Crystallogr. Sect. A*, 2004, **60**, 371-381. (b) C. Gatti, V. R. Saunders and C. J. Roetti, *Chem. Phys.* 1994, **101**, 10686-10694. (c) R. Y. De Vries, D. Feil, V. G. Tsirelson, *Acta Crystallogr. Sect. B*, 2000, **56**, 118-123.
(4) (a) R. F. W. Bader, M. T. Carroll, J. R. Cheeseman and C. Chang, *J. Am. Chem. Soc*. 1987, **109**, 7968-7979; (b) R. F. W. Bader, *Atoms-in-Molecules: A Quantum Theory*, Clarendon: Oxford, 1990.
(5) Geometrical criterion of IUCR implemented in CheckCIF service as an acceptable for hydrogen bonding, www.iucr.org.
(6) F. H. Allen, *Acta Crystallogr. Sect.B*, 2002, **58**, 380.

APPENDIX S4: Flexibility of the sulfur's torus.

The highest maxima of deformation electron density for MeTSC and SalTSC (Figure 8 in the main text) are located in the sulfur's torus. The three highest peak values for A in MeTSC range from 1.08 to 1.21 e Å^{-3} and all of them point towards the three strong N−H···S1a hydrogen bonds. The forth peak is 0.64 e Å^{-3} and it points towards weak N−H···S1a intermolecular interactions. The two most significant peaks for B in MeTSC also have very high values of 1.24 and 1.31 e Å^{-3} but they are, in contrast to A, located in the vicinity of the molecular plane. Another two peaks for molecule B (0.70 and 0.85 e Å^{-3}) are out of the molecular plane. The accumulations for SalTSC are somewhat lower and vary from 0.54 to 0.79 e Å^{-3} (four accumulations in this range). These observations illustrate the considerable flexibility of the thioureido S atom. Apart from the apparent fluctuation of electron density maxima corresponding to LPED and their ability to occupy any position within the torus, the observed inclination of the torus in the case of MeTSC can also be considered as an adjustment tendency in order to enable better interaction with the surrounding H atoms. Namely, while the torus in SalTSC is orthogonal to the C−S bond (Figure S6c), the torus in MeTSC is inclined, in comparison to the C−S bond, with one half extended towards the two strong H-bonds that are located on the same side of the molecular plane (Figure S6a,b).

As the strongest peaks in both molecules of MeTSC reach 1.08-1.31 e Å^{-3}, they are considerably higher than the deformation density of 0.59 and 0.75 e Å^{-3} found in the single accumulation corresponding to each of the free electron pairs of nitrogen atoms N1a and N1b that are additional acceptors in the same molecule. It is also evident from the previous experimental charge density studies that accumulations of deformation electron density for conventional acceptor atoms, corresponding to the free electron pairs density of O and N, are significantly weaker and quite rarely exceed 0.80 e Å^{-3}. This observation suggests that, as acceptor, the sulfur atom is able to accumulate a much larger amount of electron density available for intermolecular interactions. Importantly, those accumulations can be located in more than two points in different regions within the torus.

Contrary to the S atom, the carbonyl O atom does not show such degree of flexibility as it always displays the two highest accumulations positioned in, or very near, to the X−C(=O)−X plane (X = C, N). Such a behavior of O atom is in complete agreement with the diagram shown in the study[1] and with the classical Lewis representation of the O atom with two free electron pairs in sp^2 plane. Custelcean has also determined that, for ureido compounds, hydrogen bonding preferably occurs in the molecular plane.[2] Considering high electronegativity of the oxygen atom, and a small atomic size, it is expected that the free electron pair density of the oxygen atom is rather compact in nature and less adjustable to environment than sulfur's. Figure 8 shows that 3-4 accumulations of similar concentration, existing around the S atom, have no particular preference towards the N−C(=S)−N plane. S atom is allowed, through redistribution of electron density within the torus, to form a larger number of important interactions whose spatial arrangement is not confined by the orientation of the N−C(=S)−N plane. Thus, for example, in SalTSC (where six D−H···S interactions have been identified by the topological analysis of the total electron density) accumulations are more-less equally distributed across the toroidal arrangement as a result of sulfur's tendency to satisfy all six D−H donor groups (located all around S acceptor and directed towards it).

Another argument goes in favor of the sulfur's pronounced flexibility: S acceptors in the gas phase have nearly identical (toroidaly shaped) distribution of the negative MEP with nearly identical magnitudes (intensity) (Figure S11). However, as shown by experiments involving three molecules (A, B and SalTSC), in corresponding crystalline packings, these features (shape and magnitude), can change and deform in entirely different manners (Figure S16) as the intermolecular interactions lead to different redistributions of the "flexible" electron densities of the S pairs.

(1) P. A. Wood, E. Pidcock and F. H. Allen, *Acta Crystallogr., Sect. B*, 2008, **64**, 491−496.
(2) R. Custelcean, *Chem. Commun.*, 2008, 295-307.

APPENDIX S5: Non-bonded charge concentration within the acceptor valence shell.

The values and distribution of Laplacians of electron density in different thioureido-based molecules in gas-phase have already been analyzed in Appendix S3. The theoretical results show that accumulation of electron density in the area of S torus is quite homogeneously distributed and, interestingly enough, very much so for all 19 different thioureido molecules (Figure S10c). This similarity could be attributed to the fact that none of the S atoms have been influenced by H-bonds. The present Appendix S5 sets out only experimental results.

By investigating the topology of negative Laplacians of experimental electron density (Table S8), in cases of the three sulfur acceptors from SalTSC and MeTSC, we were able, firstly, to examine the exact disposition of (3,-3) critical points with regard to the spatial distribution of the surrounding donor groups and, secondly, to quantify the amount of density in these critical points facing towards a particular donor. It appears that the disposition of the local charge concentrations within the torus (Figure S18) is in agreement with observed features of 3D deformation electron density (Figure 8, main text) and supports the conclusions that density maxima closely follow the arrangement of intermolecular interactions and that sulfur atom is able to accommodate the requirements of the environment. In addition, the (3, –3) critical points recording the most negative Laplacians (the highest accumulations of electron density) are oriented towards the strongest N−H···S interactions regardless of their spatial distribution (position) in relation to the molecular plane.

In contrast to S atom, which can have several, differently arranged local charge concentrations placed at the average distance of 0.64 Å from the atomic core (Table S8), O atoms usually display two (3,-3) critical points that are placed in the X−C(=O)−X, (X= C, N, O) plane and are more tightly linked to the atom (about 0.3 Å).[1] It can, therefore, be suggested that O atom represents a more rigid acceptor which tends to dictate the disposition of the formed hydrogen bonds, while S is more flexible and able to adjust its acceptor surface to the requirements of the environment.

The different spatial distribution of the (3, –3) critical points in two S toruses (MeTSC), and also the variation of charge concentration in these points, demonstrate that density within the torus can easily be influenced by the present N−H···S interactions.

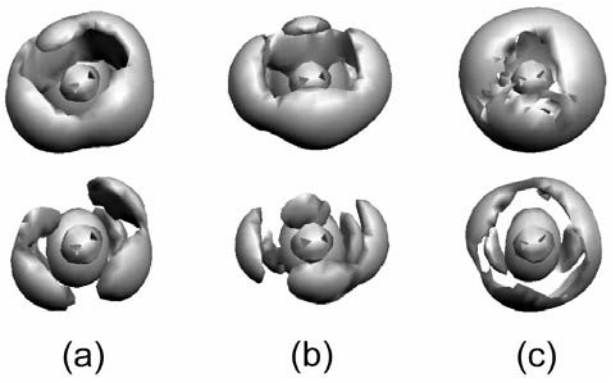

Figure S18. 3D Laplacian of the sulfur torus (viewed down the C−S bond) in molecules: (a) A, (b) B and (c) SalTSC. First row: isosurfaces at 2.40 e Å^{-5} (for SalTSC is 4.10 e Å^{-5}); Second row: isosurfaces at 7.00 e Å^{-5}. The spatial disposition of H atoms and orientation of molecular plane are the same as in Figure 5.

Table S8. Properties of (3, −3) Critical Points in the Laplacian for S atoms of MeTSC and SalTSC.

	CP	$-\nabla^2\rho_{cp}$ (e Å^{-5})	ρ_{cp} (e Å^{-3})	S···CP (Å)	CP−S−CP (º)	
MeTSC (S1a)	CP1	26.83	2.08	0.630	CP1−S−CP3	96.1
	CP2	24.02	2.04	0.634	CP2−S−CP4	93.8
	CP3	22.08	1.93	0.638	CP3−S−CP2	88.4
	CP4	12.31	1.56	0.659	CP4−S−CP1	82.6
	CP5	5.63	1.07	0.690	CP5−S−CP1	94.9
MeTSC (S1b)	CP1	28.45	2.19	0.630	CP1−S−CP3	85.8
	CP2	27.40	2.12	0.631	CP2−S−CP4	89.8
	CP3	15.94	1.68	0.652	CP3−S−CP2	92.4
	CP4	12.89	1.69	0.658	CP4−S−CP3	92.5
	CP5	4.80	1.05	0.690	CP5−S−CP1	88.8
	CP6	3.09	1.10	0.693	CP6−S−CP1	90.4
SalTSC (S1)	CP1	17.03	1.68	0.649	CP1−S−CP4	91.6
	CP2	13.58	1.56	0.661	CP2−S−CP3	76.6
	CP3	12.20	1.50	0.666	CP3−S−CP1	99.8
	CP4	12.20	1.47	0.667	CP4−S−CP2	88.8
	CP5	7.27	1.35	0.737	CP5−S−CP1	102.8

(1). B. Dittrich, R. Flaig, T. Koritsánszky, H.-G. Krane, W. Morgenroth and P.Luger, *Chem. Eur. J*. 2000, **6**, 2582-2589. (b) R. Flaig, T. Koritsanszky, R. Soyka, L. Häming and P. Luger, *Angew. Chem. Int. Ed*. 2001, **40**, 355-339; (c) C. Gatti, V. R. Saunders and C. J. Roetti, *Chem. Phys*. 1994, **101**, 10686-10696. (d) D. Parrish, E. A. Zhurova, K. Kirschbaum and A. A. Pinkerton, *J. Phys. Chem. B*, 2006, **110**, 26442-26447. (e) D. E. Hibbs, J. Overgaard and R. O. Piltz, *OrgBiomolChem*. 2003, **1**, 1191–1198; (f) D. E. Hibbs, J. R. Hanrahan, M. B. Hursthouse, D. W. Knight, J. Overgaard, P. Turner, R. O. Piltz and M. P. Waller, *Org.Biomol.Chem*. 2003, **1**, 1034–1040.

APPENDIX S6: Characterization of D−H···S (D = N, C) intermolecular interactions according to the criteria of Koch and Popelier.

The topological features of the D−H···S interactions are also evaluated trough eight following hydrogen bonding criteria established by Koch and Popelier: [1]

(1) existence of a BCP between a donor atom and an acceptor atom linked via a bond path,
(2) charge density evaluated at the BCP,
(3) Laplacian of the charge density evaluated at the BCP,
(4) mutual penetration of hydrogen and acceptor atom,
(5) loss of charge of the hydrogen atom,
(6) energetic destabilization of the hydrogen atom,
(7) decrease of dipolar polarization of the hydrogen atom,
(8) decrease of the hydrogen atom's volume.

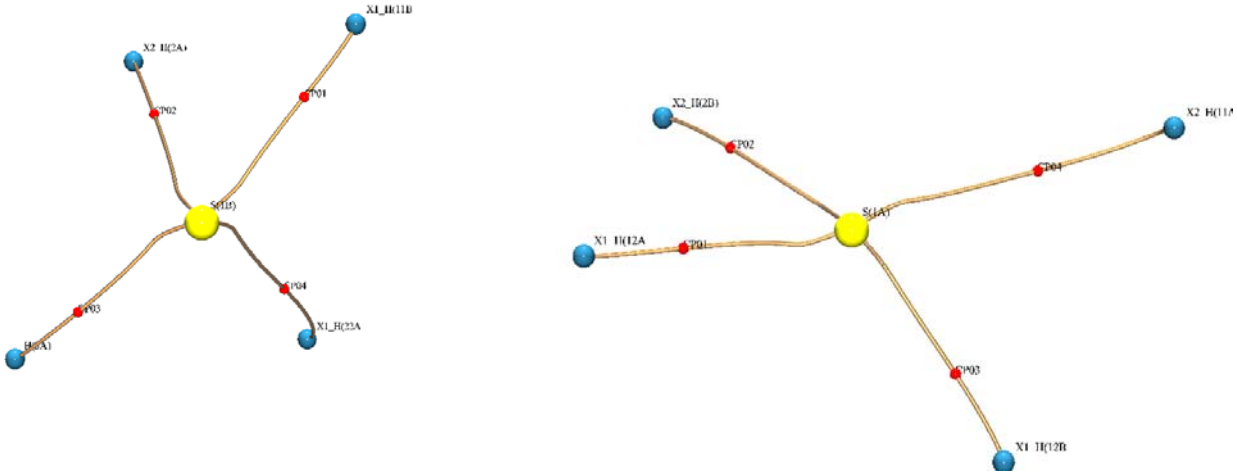

Figure S19. Molecule graph of D−H···S interactions to S1a (left) and S1b (right) acceptors. Yellow lines indicate the bond paths, while the small red spheres indicate the position of the bond critical points.

In accordance with the first necessary criterion, D−H···S interactions to each of the S atoms are characterized by the corresponding BCPs. The BCPs are, as expected, placed on the bond paths which link the H and S atoms as represented on molecule graphs (Figure S19). In all cases BCP is positioned closer to the hydrogen atom. The bond path lengths R_{ij} are indicated in the Table S9.

The values of the charge density ρ_{bcp}, required by the second condition have been determined and listed in Table 2, main text. For six N−H···S interactions with similar geometrical features ($d_{H\cdots S}$ distances ranging from 2.470(9) to 2.528(10) Å and N–H···S angles from 147.1(8) to 169.1(7)º) the density in the corresponding BCPs has rather uniform values from 0.075(13) to 0.082(13) e Å^{-3}. For two remaining weak interactions (N11–H11a···S1a and C2–H22b···S1b), ρ_{bcp} values are considerable lower (0.026(1) and 0.036(4) e Å^{-3}, respectively). The evaluated local energy densities follow the similar trend. Considering the potential energy density V_{bcp} as a quantity proportional to the hydrogen bond energy a clear separation can be observed between the values for the six stronger (from −15.65 to −19.93 kJ mol^{-1}) and two weaker hydrogen bonds (−4.86 and −6.23 kJ mol^{-1}).

The third criterion concerns $\nabla^2\rho_{bcp}$ which should have positive values, indicating the closed shell nature of the hydrogen bonding interactions. This is the case for all D−H···S interactions. The values of $\nabla^2\rho_{bcp}$ for stronger interactions are mutually close (1.04(1)−1.21(1) e Å^{-5}) and comparable to the literature data for N−H···S interactions with similar R_{ij} values.[2]

The fourth criterion of Koch and Popelier which concerns the mutual penetrations of the donor and acceptor atoms is described in more details in the main text.

Table S9. The bond paths of the D−H···S interactions and differences between the integrated properties [a] of the corresponding H atoms in the crystal system and the free molecule.

S···H	$d_{H\cdots S}$ (Å)	R_{ij}	Δq	ΔE(H)	Δμ(H)	ΔV_{001}(H)
S1a···H12a	2.528(10)	2.709	0.051	0.1329	−0.013	−4.71
S1a···H2b	2.495(9)	2.561	0.064	0.0884	−0.032	−6.47
S1a···H12b	2.501(9)	2.577	0.066	0.1142	−0.034	−6.36
S1a···H11a	3.165(9)	3.198	0.020	0.0008	−0.090	−2.29
S1b···H11b	2.470(9)	2.588	0.050	0.1330	−0.027	−4.05
S1b···H2a	2.515(10)	2.572	0.064	0.1530	−0.019	−4.82
S1b···H3a	2.517(10)	2.559	0.031	0.0358	−0.036	−5.66
S1b···H22a	2.981(11)	3.164	0.002	0.0055	−0.003	−0.90

[a]Net atomic charges (q), atomic potential energies (E), atomic dipolar polarization (μ) and volumes of the region of the atomic basin (V_{001}) where ρ(r) is greater or equal 0.001 au. Units of au.

The atomic basin properties in the gas-phase for the isolated molecule are obtained with the program package AIM2000. The calculated values are compared with the corresponding properties in the crystal determined from the experimental data by TOPXD module of XD program package. Table S9 displays the changes in the integrated properties of the H atoms after the D−H···S hydrogen bonding formation (crystal−isolated molecule). The expected trend of net charge increasing is observed for all H atoms. For stronger, similar N−H···S interactions the changes are rather consistent with exception of H3a atom where the positive charge is less increased after the hydrogen bonding. In the crystal state H atoms also display corresponding energetic destabilization (given in terms of nuclear−electron potential energy with its own nucleus) as well as the decrease of the magnitude of the atomic dipole vector. In accordance with the charge (electron) loss after the hydrogen bonds formation the decrease of the atom volumes is evident for all H atoms.

1. U. Koch, P. L. A. Popelier, *J. Phys. Chem*. 1995,**99**, 9747-9754.
2. P. Munshi, T. N. Guru Row, *CrystEngComm*, 2005, **7**, 608–611.

APPENDIX S7: Capability of acceptor to form weak hydrogen bonds.

In our previous experimental results for SalTSC we have found four C−H···S contacts with H···S distances between 3.02 and 3.12 Å. These four interactions, in addition to two N−H···S, have also been confirmed as (3, −1) critical points by a topological analysis of total electron density – a method widely accepted as relevant for analyzing hydrogen bonds. In the case of molecule B in MeTSC, one C−H···S interaction has been found and confirmed by the topological analysis and one of four electron density accumulations in the S1b torus is clearly directed towards C−H donor (Figure 5, main text). The C−H···S interactions occurring in SalTSC and MeTSC and also the interactions of this type which are, so far, topologically characterized in other experimental charge density studies[1] usually display H···S distances very close to the sum of the van der Waals' radii. The amount of electron density in corresponding BCP is rather low, and usually below 0.06 e $Å^{-3}$, (similarly to most of C−H···O and C−H···N in other experimental charge density studies[2] qualifying these interactions as very weak hydrogen bonds.

The above experimental results, together with the findings on theoretically determined MEP for various TSC molecules (Figure S11 and Appendix S3), and in combination with other factors – the evidence of the S atom spatial effect, the total mutual penetration for H and S in MeTSC and SalTSC – support the conclusions about stabilizing contribution of C−H···S interactions.

(1) (a) P. Munshi, T. S. Thakur, T. N. Guru Row and G. R. Desiraju, *Acta Crystallog. Sect.B*, 2006, **62**, 118-127. (b) R. Destro, R. Soave, M. Barzaghi and L. Lo Presti, *Chem.-Eur. J*., 2005, **11**, 4621-4534. (c) P. Munshi and T. N. Guru Row, *Acta Crystallogr., Sect. B*, 2006, **62**, 612−626; (d) D. J. Wolstenholme, J. J. Weigand, E. M. Cameron and T. S. Cameron, *Cryst. Growth Des*., 2009, **9**, 282−290; (e) D. J. Wolstenholme, J. J. Weigand, E. M. Cameron and T. S. Cameron, *Phys. Chem. Chem. Phys*. 2008, **10**, 3569−3577; (f) P. Munshi, E. Cameron, T. N. Guru Row, J. D. Ferrara and T. S. Cameron, *J. Phys. Chem. A*, 2007, **111**, 7888−7897.

(2) (a) U. Koch and P. L. A. Popelier, *J. Phys. Chem*., 1995, **99**, 9747−9754. (b) C. Gatti, E. May, R. Destro and F. Car, *J. Phys. Chem. A*, 2002, **106**, 2707-2720. (c) P. Munshi, T. N. Guru Row, *J. Phys. Chem. A*. 2005, **109**, 659-672. (d) P. R. Mallinson, G. T. Smith, C. C. Wilson, E. Grech and K. Wozniak, *J. Am. Chem. Soc*. 2003, **125**, 4259-4270.

APPENDIX S8: Sulfur's capacity (ability) to form multiple hydrogen bonds.

Prior to our previous paper[1], where we used the CSD database[2] to investigate hydrogen bonding to sulfur atom, the sulfur's ability to accept a great number of donors had, to our knowledge, not been explored. We then showed that even in more than 50% of the 835 thioureido crystal structures examined, the single S atom formed, on average, more than four D−H···S interactions (D = O, N, or C) with H···S distance below, or equal to, 3.1 Å. In present work we have repeated some parts of this analysis using an updated version of CSD database (Version 3.20, update Feb 2009). The criteria were as follows: crystallographic R factor less than 0.075, error-free coordinates (according to selected CSD criteria), and no disorder or polymerization. All the hydrogen-atom positions determined from the X-ray data were normalized to the standard neutron-derived bond distance (1.083, 1.009, and 0.983 Å for C−H, N−H, and O−H groups, respectively) along the D−H bond vector derived from the X-ray results. The structures were retained only if the H...S distances were less then 3.1 Å. This time the database produced 1617 crystal structures containing thioureido fragment and meeting the same criteria that had previously been set. It was found that more than 40% of the crystal structures contained the thioureido S atom able to engage in more than four D−H···S interactions on average, excluding those at intramolecular level.

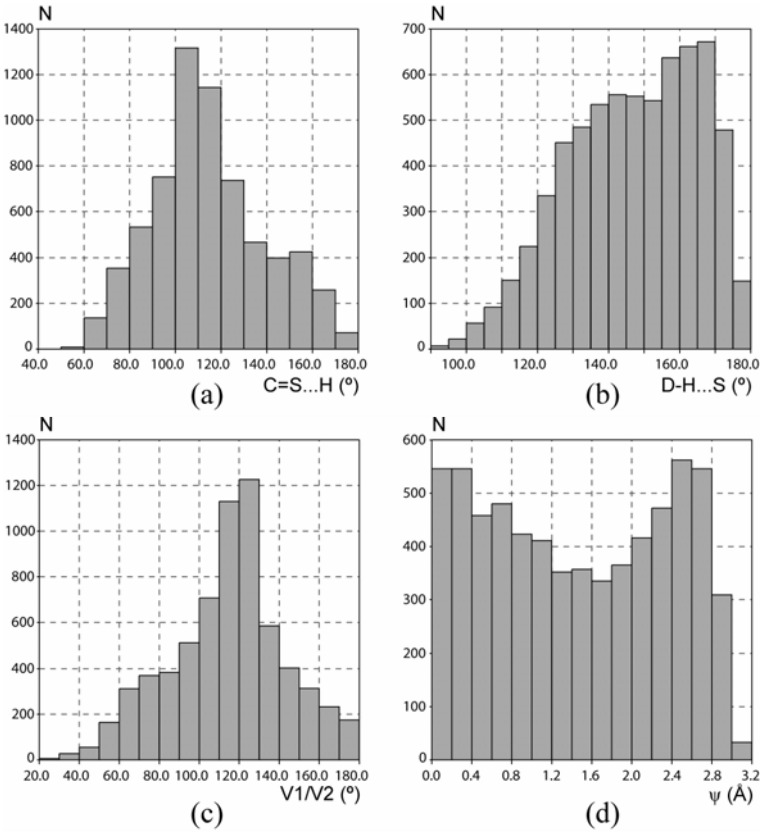

Figure S20. Distribution of the geometrical parameters (analyzed in CSD) for the D−H···S interactions: (a) C=S···H is the angle between the approaching H atom and the C=S bond; (b) D−H···S (D = O, N, C) is the angle between D−H donor group and S atom; (c) V1/V2 is the angle between the vectors directed along the D−H and C=S bonds; (d) ψ is the displacement of the hydrogen atom from the N−C(=S)−N plane. In all diagrams N represents the number of structural fragments.

As in our previous paper, the D−H···S interactions geometry confirms the space distribution pattern of the interactions that corresponds to the torus-shaped electron density of the S atom (Figure S20), confirming in this way our experimental results. The toroidal shape of the sulfur's LPED and the position of the deformation density maxima (with regard to the C−S bond) are consistent with the preferable range of C−S···H angle shown in Figure S20a. Spatial directionality of D−H donor groups (Figure S20b,d) and distribution of H atoms around the C−S bond (Figure S20c) are in agreement to experimental electron density distribution and MEP at the S atom. It is interesting to note that although there were no restrictions on the D−H···S angle during the database search, in more than 97% of 6611 S···H interactions, the angle value exceeded 110° (Figure S20b). This is an indication that the location of the H atoms in the vicinity of sulfur, at a distance shorter than 3.1 Å, is not accidental and that this position is a consequence of a stabilizing intermolecular interaction.

(1) S. B. Novaković, B. Fraisse, G. A. Bogdanović and A. Spasojević−de Biré, *Cryst. Growth Des*., 2007, **7**, 191−195.
(2) F. H. Allen, *Acta Crystallogr., Sect. B*, 2002, **58**, 380−388.

APPENDIX S9: Strength of the D−H···S interactions.

The next criterion for evaluation of the S atom acceptor capability is the strength of D−H···S in comparison to D−H···O interactions, (D = N, O, C). N−H···S and N−H···O are the most suitable for the mutual comparison. Quantitative account of the intermolecular interactions on the basis of experimental electron density distribution primarily relies on the results of the topological analysis. As expected, the values of topological parameters in corresponding BCP's: ρ_{bcp}, $\nabla^2\rho_{bcp}$ and local energy densities[1] generally indicate lower strength of N−H···S in comparison to N−H···O interactions. In the present molecules, the values of ρ_{bcp} and $\nabla^2\rho_{bcp}$ for N−H···S interactions (except for one N−H···S where H···S distance is long) vary by a narrow range from 0.063(14)-0.083(8) e Å^{-3} and 1.00(1)-1.21(1) e Å^{-5} respectively. However, even these values are comparable to topological properties of some N−H···O interactions which are classified as moderate H-bonds.[2]

On the basis of ab initio calculations Wood *et al.*[3] determined the energies of H-bonds for O and S acceptors. The calculations show that the total interaction energy of N−H···S (20.6 kJ mol^{-1}) is not far from that of N−H···O interactions of the carbonyl compounds (22.9 kJ mol^{-1}). On the other hand, it is about 2/3 of the energy calculated for N−H···O (32.8 kJ mol^{-1}) for urea-compounds containing a particularly strong O acceptor. However, although S atom forms weaker H-bonds than O atom, their total energetic stabilizing contribution is similar if we take into account that in crystal structures O forms two N−H···O on average while S forms three N−H···S.

(1) (a) E. Espinosa, E. Molins and C. Lecompte, *Chem. Phys. Lett*., 1998, **285**, 170−173; (b) P. Munshi and T. N. Guru Row, *CrystEngComm*., 2005, **7**, 608–611.
(2) (a) J. Ellena, A. E. Goeta, J. A. K. Howard and G. Punte, *J. Phys. Chem. A*, 2001, **105**, 8696-8708. (b) S. Grabowsky, T. Pfeuffer, L. Chechinska, M. Weber, W. Morgenroth, P. Luger and T. Schirmeister, *Eur. J. Org. Chem*. 2007, 2759-2768. (c) B. Dittrich, T. Koritsanszky, M. Grosche, W. Scherer, R. Flaig, A. Wagner, H. G. Krane, H. Kessler, C. Riemer, A. M. M. Schreursf and P. Luger, *Acta Crystallogr., Sect. B*, 2002, **58**, 721-727.
(3) P. A. Wood, E. Pidcock and F. H. Allen, Acta Crystallogr., Sect. B, 2008, **64**, 491−496

```
#\#CIF_1.1

#  Archive CIF produced by XD routine XDCIF
#  Created on 24-Mar-03  at 09:50:26
#  Using CIFtbx version 2.6.2 16 Jun 1998

#  Dictionary name : cif_core.dic
#  Dictionary vers : 2.3
#  Request file    : c:/WinXD/lib/xd/xdcif.dat
#  CIF files read  : geo lsm

data_publication_text
_publ_requested_journal
_publ_contact_author_name        'Goran A. Bogdanovi\'c'
_publ_contact_author_address
;
VIN\<CA Institute of Nuclear Sciences
Laboratory of Theoretical Physics and Condensed Matter Physics
PO Box 522
11001 Belgrade
Serbia
;
_publ_contact_author_email    goranb@vinca.rs
_publ_contact_author_phone    '+381 62 211 529'
_publ_contact_author_fax      '+381 11 8065829'
loop_
_publ_author_name
_publ_author_address
'Bojana M. Francuski'
;
VIN\<CA Institute of Nuclear Sciences
Laboratory of Theoretical Physics and Condensed Matter Physics
PO Box 522
11001 Belgrade
Serbia
;
'Sladjana B. Novakovi\'c'
;
VIN\<CA Institute of Nuclear Sciences
Laboratory of Theoretical Physics and Condensed Matter Physics
PO Box 522
11001 Belgrade
Serbia
;
'Goran A. Bogdanovi\'c'
;
VIN\<CA Institute of Nuclear Sciences
Laboratory of Theoretical Physics and Condensed Matter Physics
PO Box 522
11001 Belgrade
Serbia
;

_publ_requested_category         FO

 _publ_contact_letter
;
Please consider this CIF submission for publication in J.Am.Chem.Soc
I certify that all authors have seen and approved of this submission,
that all have made significant scientific contributions to the work reported,
```

```
and that all share responsibility and accountability for the results.
Goran A. Bogdanovi\'c
;

_publ_section_title
;
Electronic Features and Hydrogen Bonding Capacity of the Sulfur Acceptor in
Thioureido-based Compounds. Experimental Charge Density Study of
4-methyl-3-thiosemicarbazide
;

_publ_section_abstract
;

;
_publ_section_comment
;
;

data_tsc5

_audit_creation_date           '24-Mar-03 T09:50:26-00:00'
_audit_creation_method         'XD routine XDCIF'
_audit_conform_dict_name        cif_core.dic
_audit_conform_dict_version     2.3
_audit_conform_dict_location    ftp://ftp.iucr.org/pub/cif_core.dic

#------------------------------------------------------------------------------#
#                    CHEMICAL INFORMATION                                      #
#------------------------------------------------------------------------------#

_chemical_name_systematic
;
 ?
;
_chemical_formula_moiety                'C2 H7 N3 S1'
_chemical_formula_sum                   'C2 H7 N3 S1'
_chemical_formula_weight                105.18
_chemical_compound_source               'synthesis as described'

#------------------------------------------------------------------------------#
#                    UNIT CELL INFORMATION                                     #
#------------------------------------------------------------------------------#

_space_group_crystal_system             monoclinic
_symmetry_space_group_name_H-M           'P 21/c'
_symmetry_space_group_name_Hall          '-P 2ybc'
loop_
    _space_group_symop_id
    _space_group_symop_operation_xyz
1 +X,+Y,+Z
2 -X,1/2+Y,1/2-Z
3 -X,-Y,-Z
4 +X,1/2-Y,1/2+Z
```

```
_cell_length_a                          5.3666(2)
_cell_length_b                          8.7396(2)
_cell_length_c                          19.1354(6)
_cell_angle_alpha                       90
_cell_angle_beta                        92.854(2)
_cell_angle_gamma                       90
_cell_volume                            996.59(5)
_cell_formula_units_Z                   8
_cell_measurement_temperature           100.0(1)
_cell_measurement_reflns_used           968
_cell_measurement_theta_min             11.24
_cell_measurement_theta_max             25.13
_cell_measurement_wavelength            0.71073
#-----------------------------------------------------------------------------#
#                    CRYSTAL INFORMATION                                      #
#-----------------------------------------------------------------------------#

_exptl_crystal_description              prismatic
_exptl_crystal_colour                   colorless
_exptl_crystal_size_max                 0.32
_exptl_crystal_size_mid                 0.31
_exptl_crystal_size_min                 0.24
_exptl_crystal_density_diffrn           1.402
_exptl_crystal_density_method           'not measured'
_exptl_crystal_F_000                    448
_exptl_special_details
;
#-----------------------------------------------------------------------------#
#                    ABSORPTION CORRECTION                                    #
#-----------------------------------------------------------------------------#

_exptl_absorpt_coefficient_mu     0.496
_exptl_absorpt_correction_type    none

#-----------------------------------------------------------------------------#
#                    DATA COLLECTION                                          #
#-----------------------------------------------------------------------------#

_diffrn_ambient_temperature       100.0(1)
_diffrn_radiation_wavelength      0.71073
_diffrn_radiation_type            MoK\a
_diffrn_radiation_source          'fine-focus sealed tube'
_diffrn_radiation_monochromator   graphite
_diffrn_measurement_device_type   'Bruker SMART CCD 1K'
_diffrn_measurement_method        '\w scans'
_diffrn_reflns_number             114960
_diffrn_reflns_av_R_equivalents   0.0231
_diffrn_reflns_av_sigmaI/netI     0.0385
_diffrn_reflns_limit_h_min        -12
_diffrn_reflns_limit_h_max        12
_diffrn_reflns_limit_k_min        0
_diffrn_reflns_limit_k_max        19
_diffrn_reflns_limit_l_min        0
_diffrn_reflns_limit_l_max        42
_diffrn_reflns_theta_min          0
_diffrn_reflns_theta_max          51.43
_reflns_number_total              10401
_reflns_number_gt                 7503
_reflns_threshold_expression      >3sigma(I)
```

```
_diffrn_reflns_theta_full
_diffrn_measured_fraction_theta_full     1
_diffrn_measured_fraction_theta_max      1
#------------------------------------------------------------------------------#
#                    COMPUTER PROGRAMS USED                                    #
#------------------------------------------------------------------------------#
_computing_data_collection              'Bruker-SMART (Bruker, 2001)'
_computing_cell_refinement              'SAINT (Bruker, 2001)'
_computing_data_reduction               'SORTAV (Blessing, 1997)'
_computing_structure_solution           'WinGX program package (WinGX, 1999)'
_computing_structure_refinement
'XD2006 program package             'Volkov et al. (2006)'
_computing_publication_material         'Volkov et al. (2006)'

_publ_section_references
;
SMART (5.625), SAINT (6.02), SADABS (2.03): Data Collection and Processing
Software for the SMART System; Siemens (BRUKER-AXS) Analytical X-ray
Instruments: Madison, WI, 2001.

Blessing, R. H. (1997). J. Appl. Crystallogr. 1997, 30, 421.

WinGX (1999). Program package for structure solution,
Farrugia, L. J. J. Appl. Cryst. 1999, 32, 837.

Sheldrick, G. M. (1996). <i>SADABS</i>. University of G\"ottingen, Germany.

Sheldrick, G. M. (2008). <i>Acta Cryst.</i> A<b>64</b>, 112--122.

Volkov, A.; Macchi, P.; Farrugia, L. J.; Gatti, C.;
Mallinson, P. R.; Richter, T. and Koritsanszky, T. (2006)
XD2006 - a computer program for multipole refinement,
topological analysis and evaluation of intermolecular
energies from experimental and theoretical structure factors.
;

#------------------------------------------------------------------------------#
#                    REFINEMENT INFORMATION                                    #
#------------------------------------------------------------------------------#

_refine_special_details
;
'multipole refinement against low temperature
 high resolution X-ray diffraction data'
;
_refine_ls_structure_factor_coef        F
_refine_ls_matrix_type                  full
_refine_ls_weighting_scheme             calc
_refine_ls_weighting_details
;
        calc w1 = 1/[s^2^(Fo)]
;
_refine_ls_extinction_method            none
_refine_ls_number_reflns                7503
_refine_ls_number_parameters            437
_refine_ls_number_restraints            0
_refine_ls_R_factor_all                 0.0295
_refine_ls_R_factor_gt                  0.0178
_refine_ls_wR_factor_ref                0.0199
```

```
_refine_ls_wR_factor_gt                0.0385
_refine_ls_goodness_of_fit_ref         0.817
_refine_ls_shift/su_max                0.003
_refine_diff_density_max               0.242
_refine_diff_density_min              -0.648
_refine_diff_density_rms               0.041

#-------------------------------------------------------------------------------#
#                    ATOMIC TYPES, COORDINATES AND THERMAL PARAMETERS           #
#-------------------------------------------------------------------------------#

loop_
    _atom_site_label
    _atom_site_fract_x
    _atom_site_fract_y
    _atom_site_fract_z
    _atom_site_U_iso_or_equiv
    _atom_site_occupancy
    _atom_site_symmetry_multiplicity
S(1A) -0.005344(16) -0.312524(11) 0.768995(5) 0.014 1 4
S(1B) 0.538721(15) 0.183534(11) 0.917955(5) 0.014 1 4
N(1A) 0.54151(8) -0.05982(6) 0.75927(2) 0.019 1 4
N(2A) 0.37059(7) -0.16766(5) 0.74465(2) 0.016 1 4
N(3A) 0.20618(6) -0.08825(4) 0.843449(17) 0.013 1 4
N(1B) -0.01654(6) 0.43378(5) 0.908262(18) 0.014 1 4
N(2B) 0.16634(6) 0.34098(5) 0.890839(17) 0.015 1 4
N(3B) 0.30043(6) 0.35203(4) 1.004829(16) 0.014 1 4
C(1A) 0.20070(5) -0.17987(4) 0.788189(16) 0.012 1 4
C(2A) 0.03751(8) -0.08203(6) 0.89520(2) 0.019 1 4
C(1B) 0.32284(6) 0.29885(4) 0.940313(16) 0.012 1 4
C(2B) 0.45281(7) 0.31311(7) 1.06368(2) 0.019 1 4
H(2A) 0.375(2) -0.234(1) 0.704(1) 0.021(8) 1 4
H(3A) 0.331(2) -0.019(1) 0.847(1) 0.032(10) 1 4
H(11A) 0.544(2) 0.009(1) 0.718(1) 0.043(10) 1 4
H(12A) 0.685(2) -0.115(1) 0.764(1) 0.029(10) 1 4
H(21A) 0.105(2) -0.014(1) 0.939(1) 0.043(10) 1 4
H(22A) -0.110(2) -0.033(1) 0.873(1) 0.061(10) 1 4
H(23A) 0.001(2) -0.197(1) 0.913(1) 0.045(10) 1 4
H(2B) 0.157(1) 0.290(1) 0.846(1) 0.029(10) 1 4
H(3B) 0.170(1) 0.414(1) 1.012(1) 0.037(10) 1 4
H(11B) -0.156(1) 0.371(1) 0.907(1) 0.022(8) 1 4
H(12B) -0.038(1) 0.509(1) 0.870(1) 0.025(8) 1 4
H(21B) 0.370(2) 0.343(1) 1.110(1) 0.058(10) 1 4
H(22B) 0.615(2) 0.359(1) 1.056(1) 0.043(9) 1 4
H(23B) 0.473(2) 0.191(1) 1.064(1) 0.046(8) 1 4

loop_
    _atom_site_aniso_label
    _atom_site_aniso_U_11
    _atom_site_aniso_U_22
    _atom_site_aniso_U_33
    _atom_site_aniso_U_23
    _atom_site_aniso_U_13
    _atom_site_aniso_U_12
S(1A) 0.01533(3) 0.01208(3) 0.01361(3) 0.00062(3) -0.00161(2) -0.00286(3)
S(1B) 0.01278(3) 0.01317(3) 0.01552(3) -0.00166(3) 0.00191(2) 0.00090(3)
N(1A) 0.01487(13) 0.01976(15) 0.02150(14) -0.00464(12) 0.00495(10) -0.00382(11)
N(2A) 0.01551(12) 0.01738(14) 0.01637(11) -0.00542(10) 0.00409(9) -0.00302(10)
N(3A) 0.01250(10) 0.01293(10) 0.01259(9) -0.00165(8) 0.00076(8) -0.00054(8)
N(1B) 0.01340(11) 0.01610(12) 0.01240(10) -0.00023(9) -0.00093(8) 0.00109(9)
```

N(2B) 0.01520(12) 0.01858(13) 0.01027(9) 0.00262(8) 0.00162(8) 0.00297(10)
N(3B) 0.01438(11) 0.01793(12) 0.00981(9) -0.00073(8) -0.00099(8) 0.00347(9)
C(1A) 0.01200(10) 0.01079(10) 0.01193(9) -0.00010(8) -0.00060(7) 0.00056(8)
C(2A) 0.01803(15) 0.02212(17) 0.01712(13) -0.00408(12) 0.00512(11) -0.00229(12)
C(1B) 0.01227(10) 0.01152(10) 0.01107(9) -0.00042(7) 0.00042(7) -0.00042(8)
C(2B) 0.01772(14) 0.02743(18) 0.01295(11) 0.00121(12) -0.00293(10) 0.00390(14)

#--#
MULTIPOLE PARAMETERS
#--#
loop_
    _atom_rho_multipole_atom_label
    _atom_rho_multipole_coeff_Pv
    _atom_rho_multipole_coeff_P00
    _atom_rho_multipole_coeff_P11
    _atom_rho_multipole_coeff_P1-1
    _atom_rho_multipole_coeff_P10
    _atom_rho_multipole_coeff_P20
    _atom_rho_multipole_coeff_P21
    _atom_rho_multipole_coeff_P2-1
    _atom_rho_multipole_coeff_P22
    _atom_rho_multipole_coeff_P2-2
    _atom_rho_multipole_coeff_P30
    _atom_rho_multipole_coeff_P31
    _atom_rho_multipole_coeff_P3-1
    _atom_rho_multipole_coeff_P32
    _atom_rho_multipole_coeff_P3-2
    _atom_rho_multipole_coeff_P33
    _atom_rho_multipole_coeff_P3-3
    _atom_rho_multipole_coeff_P40
    _atom_rho_multipole_coeff_P41
    _atom_rho_multipole_coeff_P4-1
    _atom_rho_multipole_coeff_P42
    _atom_rho_multipole_coeff_P4-2
    _atom_rho_multipole_coeff_P43
    _atom_rho_multipole_coeff_P4-3
    _atom_rho_multipole_coeff_P44
    _atom_rho_multipole_coeff_P4-4
    _atom_rho_multipole_kappa
    _atom_rho_multipole_kappa_prime0
    _atom_rho_multipole_kappa_prime1
    _atom_rho_multipole_kappa_prime2
    _atom_rho_multipole_kappa_prime3
    _atom_rho_multipole_kappa_prime4
    _atom_rho_multipole_radial_slater_n0
    _atom_rho_multipole_radial_slater_zeta0
    _atom_rho_multipole_radial_slater_n1
    _atom_rho_multipole_radial_slater_zeta1
    _atom_rho_multipole_radial_slater_n2
    _atom_rho_multipole_radial_slater_zeta2
    _atom_rho_multipole_radial_slater_n3
    _atom_rho_multipole_radial_slater_zeta3
    _atom_rho_multipole_radial_slater_n4
    _atom_rho_multipole_radial_slater_zeta4
S(1A) 6.16(4) 0 -0.016(11) -0.066(11) -0.069(11) -0.201(12) 0.236(12) 0.048(11)
-0.095(12) -0.137(11) 0.064(11) 0.000(10) -0.002(10) 0.010(10) -0.007(10)
0.044(10) -0.045(10) -0.023(12) -0.019(11) 0.021(11) 0.003(11) 0.057(11)
-0.063(11) -0.059(11) -0.043(11) -0.001(11) 1.087(4)

```
1.191363 1.191363 1.191363 1.191363 1.191363 4
3.8512666666667 4 3.8512666666667 4 3.8512666666667 4 3.8512666666667 4
3.8512666666667
S(1B) 6.14(4) 0 0.032(12) -0.032(12) -0.065(13) -0.181(13) -0.219(12) 0.020(12)
-0.270(12) 0.001(11) 0.047(12) 0.007(11) 0.017(11) 0.004(11) 0.012(11) 0.020(10)
-0.014(10) 0.021(13) -0.039(12) 0.012(12) 0.095(12) -0.014(12) 0.026(12)
0.008(12) 0.058(11) -0.020(11) 1.094(4)
1.142230 1.142230 1.142230 1.142230 1.142230 4
3.8512666666667 4 3.8512666666667 4 3.8512666666667 4 3.8512666666667 4
3.8512666666667
N(1A) 5.42(9) 0 -0.151(16) -0.03(2) 0.06(2) 0.049(19) 0.030(14) 0.041(15)
-0.081(17) 0.129(15) 0.152(19) -0.072(15) 0.004(14) 0.011(16) 0.116(15)
0.061(15) -0.112(16) 0 0 0 0 0 0 0 0 0 0.978(6) 0.84112 0.84112 0.84112 0.84112
0.84112 2 3.83936 2 3.83936 2 3.83936 3 3.83936 4 3.83936
N(2A) 5.46(8) 0 0.011(15) 0.080(18) 0.07(2) 0.059(18) -0.092(13) -0.083(15)
0.023(16) -0.027(15) 0.281(19) 0.011(15) -0.002(16) 0.188(17) -0.016(16)
0.014(16) 0.057(16) 0 0 0 0 0 0 0 0 0 0.975(5) 0.83234 0.83234 0.83234 0.83234
0.83234 2 3.83936 2 3.83936 2 3.83936 3 3.83936 4 3.83936
N(3A) 5.56(9) 0 0.010(14) 0.02(2) 0.13(2) 0.05(2) 0.090(13) 0.013(15) -0.030(16)
-0.070(14) 0.26(2) 0.004(14) -0.051(17) 0.182(16) -0.009(16) 0.005(16) 0.013(16)
0 0 0 0 0 0 0 0 0 0.973(5) 0.803224 0.803224 0.803224 0.803224 0.803224 2
3.83936 2 3.83936 2 3.83936 3 3.83936 4 3.83936
N(1B) 5.47(8) 0 0.132(14) -0.01(2) 0.03(2) 0.016(17) -0.042(13) 0.047(12)
-0.075(15) -0.185(13) 0.191(17) 0.050(14) -0.032(13) 0.012(14) -0.087(14)
-0.048(14) -0.116(15) 0 0 0 0 0 0 0 0 0 0.978(5) 0.845381 0.845381 0.845381
0.845381 0.845381 2 3.83936 2 3.83936 2 3.83936 3 3.83936 4 3.83936
N(2B) 5.39(8) 0 0.009(14) 0.058(17) 0.08(2) 0.085(17) 0.071(13) -0.110(14)
0.008(15) 0.038(14) 0.259(18) 0.012(13) 0.047(15) 0.147(15) -0.031(15) 0.033(15)
0.040(15) 0 0 0 0 0 0 0 0 0 0.986(5) 0.850211 0.850211 0.850211 0.850211
0.850211 2 3.83936 2 3.83936 2 3.83936 3 3.83936 4 3.83936
N(3B) 5.38(9) 0 0.041(15) 0.00(2) 0.06(3) 0.04(2) -0.061(13) 0.021(16)
-0.109(16) -0.019(15) 0.23(2) 0.033(15) -0.028(17) 0.188(17) -0.016(16)
0.024(16) 0.029(16) 0 0 0 0 0 0 0 0 0 0.983(5) 0.798533 0.798533 0.798533
0.798533 0.798533 2 3.83936 2 3.83936 2 3.83936 3 3.83936 4 3.83936
C(1A) 4.06(8) 0 -0.013(15) -0.09(2) -0.03(2) 0.18(2) 0.078(15) 0.018(18)
-0.241(16) 0.051(14) 0.32(2) 0.019(19) -0.03(2) 0.21(2) 0.003(19) -0.001(17)
-0.035(17) 0 0 0 0 0 0 0 0 0 1.000(7) 0.882767 0.882767 0.882767 0.882767
0.882767 2 3.1762 2 3.1762 2 3.1762 3 3.1762 4 3.1762
C(2A) 4.33(18) 0 -0.15(3) 0.08(3) 0.06(3) -0.03(3) -0.03(2) -0.04(2) -0.09(2)
0.12(2) 0.27(3) -0.11(2) 0.04(2) -0.13(2) 0.20(2) -0.03(2) -0.28(3) 0 0 0 0 0 0
0 0 0 0.980(11) 0.789378 0.789378 0.789378 0.789378 0.789378 2 3.1762 2 3.1762 2
3.1762 3 3.1762 4 3.1762
C(1B) 4.24(8) 0 0.030(16) -0.04(2) -0.02(2) 0.22(2) -0.025(16) 0.000(18)
-0.304(17) -0.069(15) 0.33(2) 0.01(2) -0.01(2) 0.22(2) 0.01(2) -0.037(18)
-0.051(18) 0 0 0 0 0 0 0 0 0 0.993(7) 0.852938 0.852938 0.852938 0.852938
0.852938 2 3.1762 2 3.1762 2 3.1762 3 3.1762 4 3.1762
C(2B) 4.29(17) 0 -0.03(3) 0.12(3) 0.17(3) 0.07(2) 0.014(18) -0.015(19) -0.04(2)
0.01(2) 0.27(3) -0.04(2) 0.071(19) -0.14(2) 0.20(2) -0.11(2) -0.23(2) 0 0 0 0 0
0 0 0 0 0.991(12) 0.836582 0.836582 0.836582 0.836582 0.836582 2 3.1762 2 3.1762
2 3.1762 3 3.1762 4 3.1762
H(2A) 0.74(7) 0 0 0 0.06(2) 0 0 0 0 0 0 0 0 0 0 0 0 0 0 0 0 0 0 0 0 0 1.13(5)
1.2 1.2 1.2 1.2 1.2 0 2 1 2 2 2 3 2 4 2
H(3A) 0.43(5) 0 0 0 0.02(3) 0 0 0 0 0 0 0 0 0 0 0 0 0 0 0 0 0 0 0 0 0 1.64(11)
1.2 1.2 1.2 1.2 1.2 0 2 1 2 2 2 3 2 4 2
H(11A) 0.75(6) 0 0 0 0.13(3) 0 0 0 0 0 0 0 0 0 0 0 0 0 0 0 0 0 0 0 0 0 1.32(6)
1.2 1.2 1.2 1.2 1.2 0 2 1 2 2 2 3 2 4 2
H(12A) 0.72(7) 0 0 0 0.05(2) 0 0 0 0 0 0 0 0 0 0 0 0 0 0 0 0 0 0 0 0 0 1.23(6)
1.2 1.2 1.2 1.2 1.2 0 2 1 2 2 2 3 2 4 2
H(21A) 0.70(6) 0 0 0 0.17(3) 0 0 0 0 0 0 0 0 0 0 0 0 0 0 0 0 0 0 0 0 0 1.16(4)
1.2 1.2 1.2 1.2 1.2 0 2 1 2 2 2 3 2 4 2
```

```
H(22A) 0.94(8) 0 0 0 0.11(3) 0 0 0 0 0 0 0 0 0 0 0 0 0 0 0 0 0 0 0 0 0 0 0 0 1.16(4)
1.2 1.2 1.2 1.2 1.2 0 2 1 2 2 2 3 2 4 2
H(23A) 0.72(7) 0 0 0 0.14(3) 0 0 0 0 0 0 0 0 0 0 0 0 0 0 0 0 0 0 0 0 0 0 0 0 1.16(4)
1.2 1.2 1.2 1.2 1.2 0 2 1 2 2 2 3 2 4 2
H(2B) 0.63(6) 0 0 0 0.08(2) 0 0 0 0 0 0 0 0 0 0 0 0 0 0 0 0 0 0 0 0 0 0 0 0 1.31(6)
1.2 1.2 1.2 1.2 1.2 0 2 1 2 2 2 3 2 4 2
H(3B) 0.58(6) 0 0 0 0.09(3) 0 0 0 0 0 0 0 0 0 0 0 0 0 0 0 0 0 0 0 0 0 0 0 0 1.48(8)
1.2 1.2 1.2 1.2 1.2 0 2 1 2 2 2 3 2 4 2
H(11B) 0.84(6) 0 0 0 0.08(2) 0 0 0 0 0 0 0 0 0 0 0 0 0 0 0 0 0 0 0 0 0 0 0 0 1.14(4)
1.2 1.2 1.2 1.2 1.2 0 2 1 2 2 2 3 2 4 2
H(12B) 0.71(6) 0 0 0 0.09(2) 0 0 0 0 0 0 0 0 0 0 0 0 0 0 0 0 0 0 0 0 0 0 0 0 1.26(5)
1.2 1.2 1.2 1.2 1.2 0 2 1 2 2 2 3 2 4 2
H(21B) 0.83(6) 0 0 0 0.15(3) 0 0 0 0 0 0 0 0 0 0 0 0 0 0 0 0 0 0 0 0 0 0 0 0 1.24(4)
1.2 1.2 1.2 1.2 1.2 0 2 1 2 2 2 3 2 4 2
H(22B) 0.69(6) 0 0 0 0.10(3) 0 0 0 0 0 0 0 0 0 0 0 0 0 0 0 0 0 0 0 0 0 0 0 0 1.24(4)
1.2 1.2 1.2 1.2 1.2 0 2 1 2 2 2 3 2 4 2
H(23B) 0.80(7) 0 0 0 0.14(3) 0 0 0 0 0 0 0 0 0 0 0 0 0 0 0 0 0 0 0 0 0 0 0 0 1.24(4)
1.2 1.2 1.2 1.2 1.2 0 2 1 2 2 2 3 2 4 2



loop_
    _atom_local_axes_atom_label
    _atom_local_axes_atom0
    _atom_local_axes_ax1
    _atom_local_axes_atom1
    _atom_local_axes_atom2
    _atom_local_axes_ax2
S(1A) C(1A) Z S(1A) N(2A) Y
S(1B) C(1B) Z S(1B) N(2B) Y
N(1A) H(12A) Z N(1A) H(11A) Y
N(2A) H(2A) Z N(2A) C(1A) Y
N(3A) H(3A) Z N(3A) C(1A) Y
N(1B) H(11B) Z N(1B) H(12B) Y
N(2B) H(2B) Z N(2B) C(1B) Y
N(3B) H(3B) Z N(3B) C(1B) Y
C(1A) N(3A) Z C(1A) N(2A) Y
C(2A) H(23A) Z C(2A) H(21A) Y
C(1B) N(3B) Z C(1B) N(2B) Y
C(2B) H(22B) Z C(2B) H(21B) Y
H(2A) N(2A) Z H(2A) C(1A) Y
H(3A) N(3A) Z H(3A) C(1A) Y
H(11A) N(1A) Z H(11A) H(12A) Y
H(12A) N(1A) Z H(12A) H(11A) Y
H(21A) C(2A) Z H(21A) H(22A) Y
H(22A) C(2A) Z H(22A) H(23A) Y
H(23A) C(2A) Z H(23A) H(22A) Y
H(2B) N(2B) Z H(2B) C(1B) Y
H(3B) N(3B) Z H(3B) C(1B) Y
H(11B) N(1B) Z H(11B) H(12B) Y
H(12B) N(1B) Z H(12B) H(11B) Y
H(21B) C(2B) Z H(21B) H(23B) Y
H(22B) C(2B) Z H(22B) H(23B) Y
H(23B) C(2B) Z H(23B) H(21B) Y
```

```
#------------------------------------------------------------------------------#
#                        MOLECULAR GEOMETRY                                    #
#------------------------------------------------------------------------------#

loop_
_geom_bond_atom_site_label_1
_geom_bond_atom_site_label_2
_geom_bond_distance
_geom_bond_site_symmetry_1
_geom_bond_site_symmetry_2
_geom_bond_publ_flag
S(1A) C(1A) 1.7162(4) 1_555 1_555 yes
S(1B) C(1B) 1.7067(3) 1_555 1_555 yes
N(1A) N(2A) 1.4065(5) 1_555 1_555 yes
N(1A) H(11A) 1.001(10) 1_555 1_555 yes
N(1A) H(12A) 0.982(9) 1_555 1_555 yes
N(2A) C(1A) 1.3480(5) 1_555 1_555 yes
N(2A) H(2A) 0.977(10) 1_555 1_555 yes
N(3A) C(1A) 1.3255(4) 1_555 1_555 yes
N(3A) C(2A) 1.4476(5) 1_555 1_555 yes
N(3A) H(3A) 0.963(10) 1_555 1_555 yes
N(1B) N(2B) 1.4127(5) 1_555 1_555 yes
N(1B) H(11B) 0.994(9) 1_555 1_555 yes
N(1B) H(12B) 0.986(9) 1_555 1_555 yes
N(2B) C(1B) 1.3475(4) 1_555 1_555 yes
N(2B) H(2B) 0.975(9) 1_555 1_555 yes
N(3B) C(1B) 1.3321(4) 1_555 1_555 yes
N(3B) C(2B) 1.4521(5) 1_555 1_555 yes
N(3B) H(3B) 0.963(9) 1_555 1_555 yes
C(2A) H(21A) 1.084(12) 1_555 1_555 yes
C(2A) H(22A) 1.045(11) 1_555 1_555 yes
C(2A) H(23A) 1.086(12) 1_555 1_555 yes
C(2B) H(21B) 1.073(11) 1_555 1_555 yes
C(2B) H(22B) 1.065(11) 1_555 1_555 yes
C(2B) H(23B) 1.076(10) 1_555 1_555 yes

loop_
_geom_angle_atom_site_label_1
_geom_angle_atom_site_label_2
_geom_angle_atom_site_label_3
_geom_angle
_geom_angle_site_symmetry_1
_geom_angle_site_symmetry_2
_geom_angle_site_symmetry_3
_geom_angle_publ_flag
H(11A) N(1A) H(12A) 108.8(8) 1_555 1_555 1_555 yes
N(2A) N(1A) H(11A) 106.4(5) 1_555 1_555 1_555 yes
N(2A) N(1A) H(12A) 108.0(6) 1_555 1_555 1_555 yes
N(1A) N(2A) C(1A) 119.35(3) 1_555 1_555 1_555 yes
N(1A) N(2A) H(2A) 120.9(5) 1_555 1_555 1_555 yes
C(1A) N(2A) H(2A) 119.8(5) 1_555 1_555 1_555 yes
C(1A) N(3A) C(2A) 125.32(3) 1_555 1_555 1_555 yes
C(1A) N(3A) H(3A) 115.1(6) 1_555 1_555 1_555 yes
C(2A) N(3A) H(3A) 119.5(6) 1_555 1_555 1_555 yes
H(11B) N(1B) H(12B) 105.2(7) 1_555 1_555 1_555 yes
N(2B) N(1B) H(11B) 109.3(5) 1_555 1_555 1_555 yes
N(2B) N(1B) H(12B) 106.4(5) 1_555 1_555 1_555 yes
N(1B) N(2B) C(1B) 120.49(3) 1_555 1_555 1_555 yes
N(1B) N(2B) H(2B) 117.6(5) 1_555 1_555 1_555 yes
```

```
C(1B) N(2B) H(2B) 120.4(6) 1_555 1_555 1_555 yes
C(1B) N(3B) C(2B) 123.31(3) 1_555 1_555 1_555 yes
C(1B) N(3B) H(3B) 116.6(11) 1_555 1_555 1_555 yes
C(2B) N(3B) H(3B) 120.1(11) 1_555 1_555 1_555 yes
S(1A) C(1A) N(2A) 118.29(3) 1_555 1_555 1_555 yes
S(1A) C(1A) N(3A) 124.59(3) 1_555 1_555 1_555 yes
N(2A) C(1A) N(3A) 117.12(3) 1_555 1_555 1_555 yes
N(3A) C(2A) H(21A) 107.5(6) 1_555 1_555 1_555 yes
N(3A) C(2A) H(22A) 110.0(6) 1_555 1_555 1_555 yes
N(3A) C(2A) H(23A) 109.8(6) 1_555 1_555 1_555 yes
H(21A) C(2A) H(22A) 110.8(9) 1_555 1_555 1_555 yes
H(21A) C(2A) H(23A) 109.8(9) 1_555 1_555 1_555 yes
H(22A) C(2A) H(23A) 109.0(9) 1_555 1_555 1_555 yes
S(1B) C(1B) N(2B) 119.37(3) 1_555 1_555 1_555 yes
S(1B) C(1B) N(3B) 123.38(3) 1_555 1_555 1_555 yes
N(2B) C(1B) N(3B) 117.24(3) 1_555 1_555 1_555 yes
N(3B) C(2B) H(21B) 107.0(6) 1_555 1_555 1_555 yes
N(3B) C(2B) H(22B) 110.1(6) 1_555 1_555 1_555 yes
N(3B) C(2B) H(23B) 107.7(5) 1_555 1_555 1_555 yes
H(21B) C(2B) H(22B) 118.4(8) 1_555 1_555 1_555 yes
H(21B) C(2B) H(23B) 107.1(8) 1_555 1_555 1_555 yes
H(22B) C(2B) H(23B) 106.0(8) 1_555 1_555 1_555 yes

loop_
_geom_torsion_atom_site_label_1
_geom_torsion_atom_site_label_2
_geom_torsion_atom_site_label_3
_geom_torsion_atom_site_label_4
_geom_torsion
_geom_torsion_site_symmetry_1
_geom_torsion_site_symmetry_2
_geom_torsion_site_symmetry_3
_geom_torsion_site_symmetry_4
_geom_torsion_publ_flag
H(2A) N(2A) C(1A) S(1A) -0.7(7) 1_555 1_555 1_555 1_555 yes
H(2A) N(2A) C(1A) N(3A) 178.9(7) 1_555 1_555 1_555 1_555 yes
N(1A) N(2A) C(1A) S(1A) -180.0(1) 1_555 1_555 1_555 1_555 yes
N(1A) N(2A) C(1A) N(3A) -0.4(1) 1_555 1_555 1_555 1_555 yes
C(2A) N(3A) C(1A) S(1A) -1.8(1) 1_555 1_555 1_555 1_555 yes
C(2A) N(3A) C(1A) N(2A) 178.65(4) 1_555 1_555 1_555 1_555 yes
H(3A) N(3A) C(1A) S(1A) -179.1(7) 1_555 1_555 1_555 1_555 yes
H(3A) N(3A) C(1A) N(2A) 1.4(7) 1_555 1_555 1_555 1_555 yes
C(1A) N(3A) C(2A) H(21A) 168.7(7) 1_555 1_555 1_555 1_555 yes
C(1A) N(3A) C(2A) H(22A) -70.5(7) 1_555 1_555 1_555 1_555 yes
C(1A) N(3A) C(2A) H(23A) 49.4(7) 1_555 1_555 1_555 1_555 yes
H(3A) N(3A) C(2A) H(21A) -14.2(10) 1_555 1_555 1_555 1_555 yes
H(3A) N(3A) C(2A) H(22A) 106.6(10) 1_555 1_555 1_555 1_555 yes
H(3A) N(3A) C(2A) H(23A) -133.5(10) 1_555 1_555 1_555 1_555 yes
H(11A) N(1A) N(2A) C(1A) -121.9(6) 1_555 1_555 1_555 1_555 yes
H(11A) N(1A) N(2A) H(2A) 58.9(9) 1_555 1_555 1_555 1_555 yes
H(12A) N(1A) N(2A) C(1A) 121.5(6) 1_555 1_555 1_555 1_555 yes
H(12A) N(1A) N(2A) H(2A) -57.8(9) 1_555 1_555 1_555 1_555 yes
H(2B) N(2B) C(1B) S(1B) 13.1(7) 1_555 1_555 1_555 1_555 yes
H(2B) N(2B) C(1B) N(3B) -167.6(7) 1_555 1_555 1_555 1_555 yes
N(1B) N(2B) C(1B) S(1B) 178.7(1) 1_555 1_555 1_555 1_555 yes
N(1B) N(2B) C(1B) N(3B) -2.0(1) 1_555 1_555 1_555 1_555 yes
C(2B) N(3B) C(1B) S(1B) -2.3(1) 1_555 1_555 1_555 1_555 yes
C(2B) N(3B) C(1B) N(2B) 178.4(1) 1_555 1_555 1_555 1_555 yes
H(3B) N(3B) C(1B) S(1B) -178.4(7) 1_555 1_555 1_555 1_555 yes
```

```
H(3B) N(3B) C(1B) N(2B) 2.3(7) 1_555 1_555 1_555 1_555 yes
C(1B) N(3B) C(2B) H(21B) -168.8(7) 1_555 1_555 1_555 1_555 yes
C(1B) N(3B) C(2B) H(22B) 66.2(7) 1_555 1_555 1_555 1_555 yes
C(1B) N(3B) C(2B) H(23B) -48.9(6) 1_555 1_555 1_555 1_555 yes
H(3B) N(3B) C(2B) H(21B) 12.1(9) 1_555 1_555 1_555 1_555 yes
H(3B) N(3B) C(2B) H(22B) -117.9(10) 1_555 1_555 1_555 1_555 yes
H(3B) N(3B) C(2B) H(23B) 127.0(9) 1_555 1_555 1_555 1_555 yes
H(11B) N(1B) N(2B) C(1B) -108.2(6) 1_555 1_555 1_555 1_555 yes
H(11B) N(1B) N(2B) H(2B) 57.8(9) 1_555 1_555 1_555 1_555 yes
H(12B) N(1B) N(2B) C(1B) 138.7(6) 1_555 1_555 1_555 1_555 yes
H(12B) N(1B) N(2B) H(2B) -55.3(9) 1_555 1_555 1_555 1_555 yes
```